JOC Article

Supramolecular Chirogenesis in Zinc Porphyrins: Interaction with Bidentate Ligands, Formation of Tweezer Structures, and the Origin of Enhanced Optical Activity

Victor V. Borovkov,*,† Juha M. Lintuluoto,‡ Guy A. Hembury,† Makiko Sugiura,§ Ryuichi Arakawa,|| and Yoshihisa Inoue*,†

Entropy Control Project, ICORP, JST, 4-6-3 Kamishinden, Toyonaka-shi, Osaka 560-0085, Japan, Kobe Pharmaceutical University, 4-19-1 Motoyamakita-machi, Higashinada-ku, Kobe 658-8558, Japan, and Department of Applied Chemistry, Kansai University, Suita, Osaka 564-8680, Japan

victrb@inoue.jst.go.jp; inoue@chem.eng.osaka-u.ac.jp

Received June 12, 2003

The complexation behavior, binding properties, and spectral parameters of supramolecular chirality induction in the achiral host molecule, syn (face-to-face conformation) ethane-bridged bis(zinc porphyrin), upon interaction with chiral bidentate guests (diamines and amino alcohols) have been studied by means of UV−vis, CD, fluorescence, ^{1}H NMR, and ESI MS techniques. It was found that the guest structure plays a decisive role in the chirogenesis pathway. The majority of bidentate ligands (except those geometrically unsuitable) exhibit two major equilibria steps: the first guest ligation leading to formation of the 1:1 host−guest tweezer structure (K_1) and the second guest molecule ligation (K_2) forming the anti bis-ligated species (1:2). The second ligation is much weaker ($K_1 \gg K_2$) due to the optimal geometry and stability of the 1:1 tweezer complex. The enhanced conformational stability of the tweezer complex ensures an efficient chirality transfer from the chiral guest to the achiral host, consequently inducing a remarkably high optical activity in the bis-porphyrin.

Introduction

Thus far, supramolecular chirogenesis has attracted much attention in the scientific community and has become a fast growing interdisciplinary field of chemistry due to its vital importance in many natural and artificial systems, its requirement for addressing many fundamental science issues, and as a basis for numerous modern molecular technologies.[1] This phenomenon is associated with the processes of chirality information transfer (and/or amplification) through noncovalent interactions in various molecular or supramolecular assemblies. Porphyrins and related chromophores are molecules of particular interests for the detailed investigation and further applications of supramolecular chirogenesis owing to their unique spectral and physicochemical properties, easy handling and versatile synthetic modifications, great biological importance, and wide applicability.

Recently, it was found that bis(zinc octaethylporphyrin)[2] (see *syn*-**1** in Figure 1) serves as an effective achiral host molecule for monodentate guests (amines and alcohols), forming 1:2 host−guest complexes in an extended anti form (*anti*-**1**·$\mathbf{L}_2$)[3] whose spectral properties are remarkably different from those of the initial *syn*-**1**, thus allowing its use for molecular recognition purposes. In the case of chiral ligands, besides syn-to-anti conformational switching, there is another type of structural deformation in **1** resulting in the generation of a chiral screw structure via a steric repulsion mechanism.[4] Specifically, the mechanism of the chirogenesis process is based on repulsive interactions between the bulkiest substituent at the stereogenic center closest to the binding site of the chiral ligand and one of the ethyl groups of the neighboring porphyrin ring (at the 3- or

* To whom correspondence should be addressed.
† ICORP, JST.
‡ Present address: Department of Synthetic and Biological Chemistry, Graduate School of Engineering, Kyoto University, Kyoto 606-8502, Japan.
§ Kobe Pharmaceutical University.
|| Kansai University.

(1) Recent examples of supramolecular chirogenesis in various systems: (a) Borovkov, V. V.; Harada, T.; Hembury, G. A.; Inoue, Y.; Kuroda, R. *Angew. Chem., Int. Ed.* **2003**, *42*, 1746−1749. (b) Ishikawa, M.; Maeda, K.; Yashima, E. *J. Am. Chem. Soc.* **2002**, *124*, 7448. (c) Nabeshima, T.; Hashiguchi, A.; Saiki, T.; Akine, S. *Angew. Chem., Int. Ed.* **2002**, *41*, 481. (d) Ribó, J. M.; Crusats, J.; Sagués, F.; Claret, J.; Rubires, R. *Science* **2001**, *292*, 2063. (e) Nakashima, H.; Koe, J. R.; Torimitsu, K.; Fujiki, M. *J. Am. Chem. Soc.* **2001**, *123*, 4847. (f) Iarossi, D.; Mucci, A.; Parenti, F.; Schenetti, L.; Seeber, R.; Zanardi, C.; Forni, A.; Tonelli, M. *Chem. Eur. J.* **2001**, *7*, 676. (g) de Loos, M.; van Esch, J.; Kellogg, R. M.; Feringa, B. L. *Angew. Chem., Int. Ed.* **2001**, *40*, 613. (h) Steffen, W.; Kohler, B.; Altmann, M.; Scherf, U.; Stitzer, K.; zur Loye, H.-C.; Bunz, U. H. F. *Chem. Eur. J.* **2001**, *7*, 117. (i) Jung, J. H.; Kobayashi, H.; Masuda, M.; Shimizu, T.; Shinkai, S. *J. Am. Chem. Soc.* **2001**, *123*, 8785. (j) Brunsveld, L.; Meijer, E. W.; Prince, R. B.; Moore, J. S. *J. Am. Chem. Soc.* **2001**, *123*, 7978. (k) Zahn, S.; Proni, G.; Spada, G. P.; Canary, J. W. *Chem. Eur. J.* **2001**, *7*, 88. (l) Rivera, J. M.; Martín, T.; Rebek, J., Jr. *Science* **2000**, *289*, 606. (m) Wang, M.; Silva, G. L.; Armitage, B. A. *J. Am. Chem. Soc.* **2000**, *122*, 9977.

(2) (a) Borovkov, V. V.; Lintuluoto, J. M.; Inoue, Y. *Synlett* **1998**, 768. (b) Borovkov, V. V.; Lintuluoto, J. M.; Inoue, Y. *Helv. Chim. Acta* **1999**, *82*, 919.

(3) (a) Borovkov, V. V.; Lintuluoto, J. M.; Inoue, Y. *Tetrahedron Lett.* **1999**, *40*, 5051. (b) Borovkov, V. V.; Lintuluoto, J. M.; Inoue, Y. *J. Phys. Chem. B* **1999**, *103*, 5151.

10.1021/jo034814k CCC: $25.00
Published on Web 08/20/2003

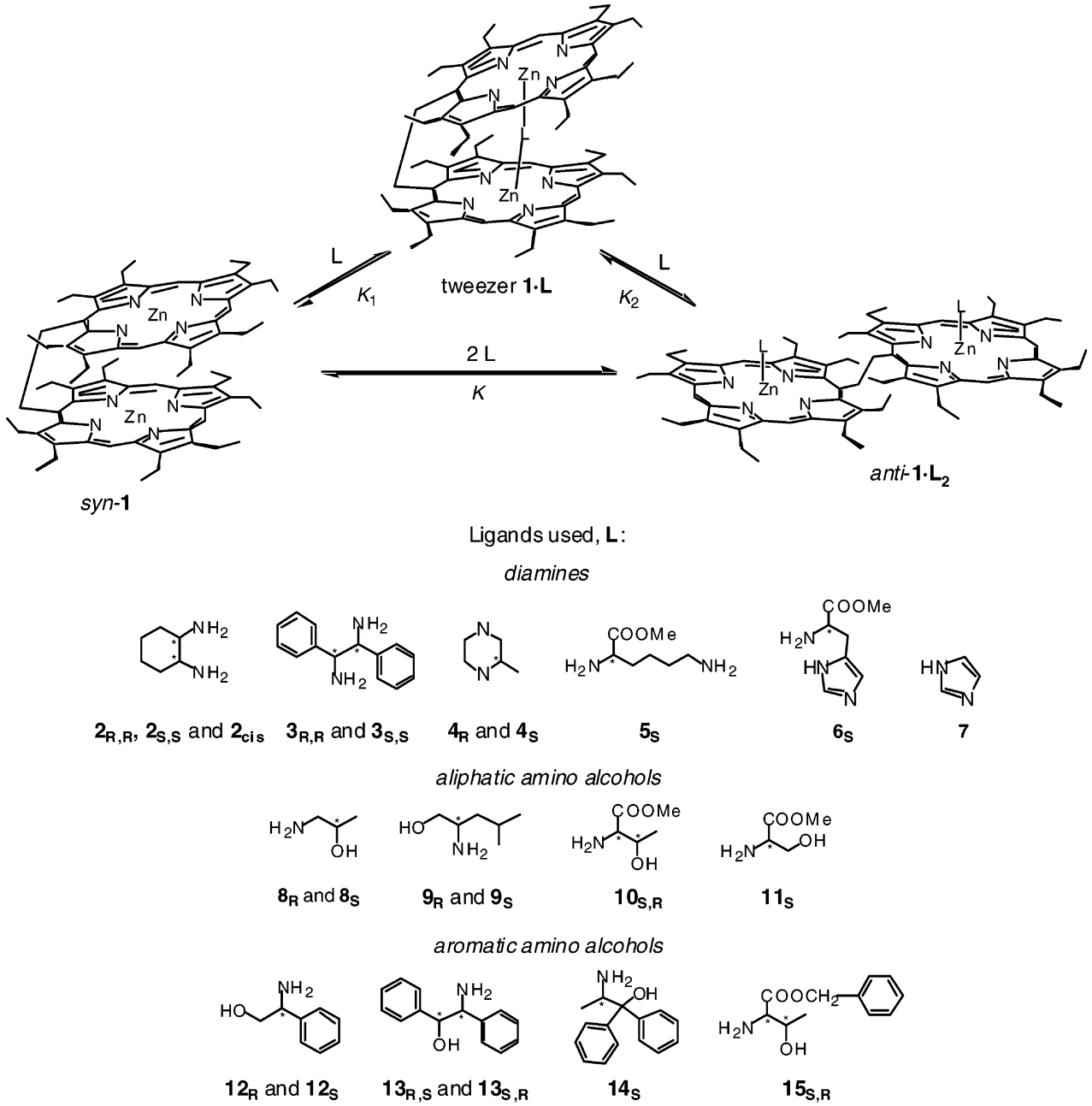

FIGURE 1. Structures and equilibria of achiral dimeric host **1** in the presence of the bidentate guests (**L**: **2**−**15**). The subscript R or S indicates the absolute configuration of the asymmetric carbon (marked by asterisk) which is the closest to the amine (and hydroxyl in the case of amino alcohols) binding groups. The subscript cis indicates the cis orientation of two amines in **2**.

7-position depending on the absolute configuration of the ligand). Hence, the direction of helical sense is governed by the position of the largest group. If the order of the substituents' bulkiness at the asymmetric carbon coincides with the priority rule according to the Cahn−Ingold−Prelog system for absolute configuration assignment, (*S*)-ligands induce the right-handed screw structure while (*R*)-ligands produce the left-handed screw, corresponding to positive and negative chirality, respectively. In the case of discordance between the bulkiness order and the priority rule, as expected, the chirality sign becomes opposite. Thus, using these regularities, simple and effective chirality sensors for monodentate ligands have been developed on the basis of *syn*-**1**[4] and the corresponding bis(magnesium porphyrin) complex.[5]

However, preliminary studies of the complexation behavior of *syn*-**1** with several diamines revealed that besides the well-known and fully characterized *anti*-**1**·

(4) (a) Borovkov, V. V.; Harada, T.; Inoue, Y.; Kuroda, R. *Angew. Chem., Int. Ed.* **2002**, *41*, 1378. (b) Borovkov, V. V.; Lintuluoto, J. M.; Sugeta, H.; Fujiki, M.; Arakawa, R.; Inoue, Y. *J. Am. Chem. Soc.* **2002**, *124*, 2993. (c) Borovkov, V. V.; Lintuluoto, J. M.; Inoue, Y. *J. Am. Chem. Soc.* **2001**, *123*, 2979. (d) Borovkov, V. V.; Yamamoto, N.; Lintuluoto, J. M.; Tanaka, T.; Inoue, Y. *Chirality* **2001**, *13*, 329. (e) Borovkov, V. V.; Lintuluoto, J. M.; Fujiki, M.; Inoue, Y. *J. Am. Chem. Soc.* **2000**, *122*, 4403. (f) Borovkov, V. V.; Lintuluoto, J. M.; Inoue, Y. *Org. Lett.* **2000**, *2*, 1565. (g) Borovkov, V. V.; Lintuluoto, J. M.; Inoue, Y. *J. Phys. Chem. A* **2000**, *104*, 9213.

(5) Lintuluoto, J. M.; Borovkov, V. V.; Inoue, Y. *J. Am. Chem. Soc.* **2002**, *124*, 13676.

TABLE 1. Observed UV−vis and CD Spectral Data of the Supramolecular Systems (1·L and 1·L$_2$) with Different Bidentate Ligands[a]

	1:1 tweezer complex(**1·L**)[b]				1:2 anti complex(**1·L$_2$**)[c]			
	UV−vis data λ (nm)	CD data λ (nm) [$\Delta\epsilon$ ($M^{-1}cm^{-1}$)]			UV−vis data λ (nm)		CD data[d] λ (nm) [sign]	
ligand (**L**)	B transitions	first Cotton	second Cotton	A_{obs}[e]	$B_{\|\|}$ transition	$B_{\perp}$ transition	first Cotton	second Cotton
2$_{R,R}$	410, 418 (sh), 436 (sh)	436 [−352]	409 [+240]	−592				
2$_{S,S}$	410, 418 (sh), 436 (sh)	436 [+348]	409 [−239]	+587				
2$_{cis}$	410, 419 (sh), 436 (sh)				438	427		
3$_{R,R}$	411, 419 (sh), 437 (sh)	438 [+207]	414 [−96]	+303	437	423	434 [−]	408 [+]
3$_{S,S}$	411, 419 (sh), 437 (sh)	438 [−205]	415 [+92]	−297	437	423	433 [+]	408 [−]
4$_R$					438	426	437 [−]	424 [+]
4$_S$					438	426	437 [+]	423 [−]
5$_S$	411, 422 (sh), 435 (sh)	436 [+301]	412 [−254]	+555	436	425	436 [+]	412 [−]
6$_S$	412, 423 (sh), 435 (sh)	436 [+319]	411 [−213]	+532	437	426	436 [+]	412 [−]
7	412, 423 (sh), 436 (sh)				437	426		
8$_R$	408, 416 (sh), 435 (sh)	435 [−232]	407 [+162]	−394	437	424	437 [−]	411 [+]
8$_S$	408, 416 (sh), 435 (sh)	435 [+237]	406 [−152]	+389	437	424	436 [+]	412 [−]
9$_R$	407, 418 (sh), 436 (sh)	435 [−271]	407 [+199]	−470	436	425	435 [−]	407 [+]
9$_S$	407, 418 (sh), 436 (sh)	435 [+275]	407 [−184]	+459	436	425	435 [+]	407 [−]
10$_{S,R}$	407, 418 (sh), 435 (sh)	432 [−16]	407 [+18]	−34	436	425	438 [+]	424 [−]
11$_S$	407, 420 (sh), 435 (sh)	434 [−100]	406 [+59]	−159	436	423	436 [−]	422 [+]
12$_R$	407, 418 (sh), 434 (sh)	433 [−218]	406 [+149]	−367	435	424	433 [−]	406 [+]
12$_S$	407, 418 (sh), 434 (sh)	433 [+220]	407 [−152]	+372	435	424	433 [+]	407 [−]
13$_{R,S}$					437	426	439 [+]	425 [−]
13$_{S,R}$					437	426	439 [−]	425 [+]
14$_S$					436	426	437 [+]	424 [−]
15$_{S,R}$	411, 422 (sh), 435 (sh)	436 [+212]	411 [−141]	+353	436	425	437 [+]	412 [−]

[a] $C_1 = (2.7-4.1) \times 10^{-6}$ M, in CH_2Cl_2. [b] The observed spectral parameters of **1·**L were determined at the corresponding maximum concentration as described in the Experimental Section. [c] The observed spectral parameters of **1·**L$_2$were determined at the saturated ligand concentration ($C_L = 10^{-2}-10^{-1}$ M) as described in the Experimental Section. [d] In the case of **1·**L formation, due to the difference in the binding constants (see Table 2) the total equilibria cannot be fully shifted toward the **1·**L$_2$ species; thus, the corresponding $\Delta\epsilon$ and A values are not shown. [e] $A_{obs} = \Delta\epsilon_1 - \Delta\epsilon_2$. This value represents the total amplitude of the experimentally observed CD couplets. The CD recording accuracy based on the baseline evaluation is ± 3 M^{-1} cm^{-1}.

L$_2$ species, a new chiral tweezer-like supramolecular structure (**1·L**) may be formed (Figure 1).[6] In general, a supramolecular tweezer is defined as a specially shaped type of 1:1 host−guest complexes arising from the insertion of a guest molecule between two binding sites of a molecular host through various noncovalent interactions, which leads to a fascinating spatial architecture, resembling a pincer holding an object. Bis-porphyrin derivatives linked by a single covalent tether are well suited to serve as host compounds for the tweezer structures owing to their unique physicochemical properties. Particularly, these include a marked difference between the spectroscopic characteristics of the corresponding host and guest components, allowing easy monitoring of the complexation process. The well-known coordination and $\pi-\pi$ stacking properties of metallo- and free base porphyrins also significantly expand the possible range of guest compounds. Although only a few chiral complexes of bis-porphyrin based tweezers have been reported so far,[7,8] they are of prime interest not only due to their sophisticated molecular design but also due to diverse practical applications in the fields of molecular and enantioselective recognition,[7d,e,g] chiral memory elements,[7a] and absolute configuration determination.[7b,c]

To investigate and describe comprehensively this interesting chirogenic phenomenon of tweezer formation, we report here systematic studies of the interaction of *syn*-**1** with various bidentate ligands (diamines and amino alcohols), detailed characterization of the resulting complex **1·L**, and roles of different controlling factors as investigated by UV−vis, CD, fluorescence, ^{1}H NMR, and ESI MS spectral techniques.

Experimental Section

Materials. The syn conformer of host **1**, in which the two porphyrin planes are fixed in a face-to-face orientation (see Figure 1), was synthesized according to previously reported methods.[2] Diamines **2**−**4** and **7**, amino alcohols **8**, **9**, and **12**−**14**, anhydrous CH_2Cl_2 for UV−vis, fluorescence, and CD measurements, and $CDCl_3$ for ^{1}H NMR and ESI MS studies

(6) For a preliminary account of this part of the work, see: (a) Borovkov, V. V.; Lintuluoto, J. M.; Sugiura, M.; Inoue, Y.; Kuroda, R. *J. Am. Chem. Soc.* **2002**, *124*, 11282. (b) Borovkov, V. V.; Lintuluoto, J. M.; Inoue, Y. *Org. Lett.* **2002**, *4*, 169.

(7) Chiral supramolecular tweezers on the basis of bis-porphyrin derivatives: (a) Kubo, Y.; Ohno, T.; Yamanaka, J.-i.; Tokita, S.; Iida, T.; Ishimaru, Y. *J. Am. Chem. Soc.* **2001**, *123*, 12700. (b) Kurtan, T.; Nesnas, N.; Li, Y.-Q.; Huang, X.; Nakanishi, K.; Berova, N. *J. Am. Chem. Soc.* **2001**, *123*, 5962. (c) Takeuchi, M.; Imada, T.; Shinkai, S. *Bull. Chem. Soc. Jpn.* **1998**, *71*, 1117. (d) Sessler, J. L.; Andrievsky, A.; Kral, V.; Lynch, V. *J. Am. Chem. Soc.* **1997**, *119*, 9385. (e) Hayashi, T.; Nonoguchi, M.; Aya, T.; Ogoshi, H. *Tetrahedron Lett.* **1997**, *38*, 1603. (f) Ema, T.; Misawa, S.; Nemugaki, S.; Sakai, T.; Utaka, M. *Chem. Lett.* **1997**, 487. (g) Crossley, M. J.; Mackay, L. G.; Try, A. C. *J. Chem. Soc., Chem. Commun.* **1995**, 1925.

(8) Achiral supramolecular tweezers on the basis of bis-porphyrin derivatives: (a) Pistorio, B. J.; Chang, C. J.; Nocera, D. G. *J. Am. Chem. Soc.* **2002**, *124*, 7884. (b) Gomila, R. M.; Quiñonero, D.; Rotger, C.; Garau, C.; Frontera, A.; Ballester, P.; Costa, A.; Deyà, P. M. *Org. Lett.* **2002**, *4*, 169. (c) Brettar, J.; Gisselbrecht, J.-P.; Gross, M.; Solladié, N. *Chem. Commun.* **2001**, 733. (d) Sun, D.; Tham, F. S.; Reed, C. A.; Chaker, L.; Burgess, M.; Boyd, P. D. W. *J. Am. Chem. Soc.* **2000**, *122*, 10704. (e) Sirish, M.; Schneider, H.-J. *J. Am. Chem. Soc.* **2000**, *122*, 5881. (f) Johnston, M. R.; Gunter, M. J.; Warrener, R. N. *Chem. Commun.* **1998**, 2739. (g) de Miguel, Y. R.; Bampos, N.; de Silva, K. M. N.; Richards, S. A.; Sanders, J. K. M. *Chem. Commun.* **1998**, 2267. (h) Imahori, H.; Yoshizawa, E.; Yamada, K.; Hagiwara, K.; Okada, T.; Sakata, Y. *J. Chem. Soc., Chem. Commun.* **1995**, 1133. (i) Naruta, Y.; Sawada, N.; Tadokoro, M. *Chem. Lett.* **1994**, 1713. (j) Collman, J. P.; Hutchison, J. E.; Lopez, M. A.; Guilard, R. *J. Am. Chem. Soc.* **1992**, *114*, 8066. (k) Tabushi, I.; Kugimiya, S.-i.; Kinnaird, M. G.; Sasaki, T. *J. Am. Chem. Soc.* **1985**, *107*, 4192.

TABLE 2. Binding and CD Spectral Data of the Supramolecular Systems (1·L and 1·L$_2$) with Different Bidentate Ligands[a]

	binding constants[b]				calculated CD data A_{calc}[d] (M^{-1} cm^{-1})	
ligand (**L**)	K_1 (M^{-1})	K_2 (M^{-1})	K (M^{-2})	Gibbs free energy $\Delta G°$ at 292 K[c](kcal mol^{-1})	1:1 tweezer complex (**1·L**)	1:2 anti complex (**1·L$_2$**)
2$_{R,R}$	1.25×10^7			−9.5	−589	
2$_{S,S}$	1.25×10^7			−9.5	+580	
2$_{cis}$	1.00×10^4	3.80×10^3		−10.1		
3$_{R,R}$	1.44×10^7	1.10×10^3		−13.6	+304	−145
3$_{S,S}$	1.44×10^7	1.10×10^3		−13.6	−230	+106
4$_R$			5.64×10^6	−9.0		−9.7
8$_R$	2.99×10^3	10		−6.0	−522	−0.5
8$_S$	2.99×10^3	10		−6.0	+465	+1.1
9$_R$	7.16×10^3	55		−7.5	−545	−213
9$_S$	7.16×10^3	58		−7.5	+519	+214
12$_R$	5.40×10^2	13		−5.0	−501	−301
12$_S$	5.40×10^2	11		−5.0	+495	+305
13$_{R,S}$			$1.56 \cdot 10^4$	−5.6		−102
13$_{S,R}$			$1.31 \cdot 10^4$	−5.5		+158
14$_S$			$3.31 \cdot 10^3$	−4.7		+197

[a] $C_1 = (2.7-4.1) \times 10^{-6}$ M, in CH_2Cl_2. [b] The standard deviation are within ±10%. [c] $\Delta G° = -RT \ln(K_1)$, $\Delta G° = -RT \ln(K_1K_2)$, or $\Delta G° = -RT \ln(K)$, where $T = 292$ K. [d] Calculated total amplitude of the CD couplets: $A_{calc} = \Delta\epsilon_{1calc} - \Delta\epsilon_{1calc}$ (see the Experimental Section).

were purchased from Fluka Chemica AG and Aldrich Chemical Co. and used as received. Amino acid derivatives **5**, **6**, **10**, **11**, and **15** have been obtained from the corresponding hydrochloride salts purchased from Kokusan Chemical Works, Ltd., Wako Pure Chemical Industries, Ltd., and BACHEM AG according to the reported procedure.[4d]

Spectroscopic Measurements. CD scanning conditions were as follows: scanning rate = 50 nm per min, bandwidth = 1 nm, response time = 0.5 s, accumulations = 1 scan. The ligand concentrations used for determination of the observed UV−vis and CD parameters of **1·L** were the concentrations where the spectral changes associated with the porphyrin chromophores of the **1·L** species were at their maximum, and a further increase of the ligand concentration resulted in a decrease of the corresponding spectral intensities due to shifting the overall equilibrium to the *anti*-**1·L$_2$** species. The saturated ligand concentrations used for the UV−vis and CD measurements were the concentrations where the spectral changes associated with the porphyrin chromophores were at maximum, and a further increase of the ligand concentration had no effect on the signal intensities (for the ligand and porphyrin concentration ranges, see footnotes a and c in Table 1).

Steady-state fluorescence scanning conditions were as follows: correction for the spectral response of the instrument, excitation, and emission slit widths = 5 nm, excitation wavelength at the maximum for the corresponding porphyrin B (Soret) band. CPF scanning conditions were as follows: excitation wavelength = 409 nm, scanning rate = 50 nm per min, excitation slit width = 3 mm, emission bandwidth = 15 nm, response time = 2 s, accumulations = 32 scan, PM voltage = 770 V.

Fluorescence decay kinetics profiles were obtained on a streak scope upon excitation by a Ti:Sapphire laser at 400 nm. The monitoring wavelength regions were 620−630 nm and 675−685 nm for **1** and 597−617 nm and 645−665 nm for **1·2$_{R,R}$**.

^{1}H NMR spectra were recorded at room temperature. Chemical shifts were referenced to the residual proton resonance in $CDCl_3$ (δ 7.25 ppm). For the ^{1}H−^{1}H ROESY experiments, the sample of **1·2$_{R,R}$** was dissolved in $CDCl_3$ and the solution was degassed and sealed under vacuum; the mixing time was set at 200 ms. The nonselective relaxation time (T_1, T_1^{NS}) was obtained using the conventional inversion−recovery (180° − τ − 90°) method. For the measurement of selective noninversion relaxation time (T_1, T_1^{SNI}), the pulse sequence (see Figure S1, Supporting Information) was applied where a selective shaped 180° pulse of i-SNOB-3 (inversion type of selective excitation for biochemical applications)[9a] was used for the achievement of the selective noninversion condition. The pulse length adopted was 23 and 5.8 μs for 90° pulses at 200 and 500 MHz, respectively, and 270−100 ms (depending on the bandwidth) for 180° pulse in the i-SNOB-3 shaped pulse experiment. For all T_1 measurements, 16 τ values (the waiting times) were included in the analysis of the data, based on the initial slope of a plot of $\ln(M_\infty - M_\tau)$ vs τ. The error for an exponential curve fitting was less than 3%. All the reported T_1 values were obtained as averages from three or four repeated experiments. The precision for the measurement of ^{1}H T_1 is less than ± 2%.

The sample solutions for ESI MS spectra at room temperature were infused directly into the mass spectrometer at a rate of 3 mL/min with the spray voltage of 4.5 kV. The resulting small particles were introduced into a heated capillary for desolvation, temperature of which was varied from 343 to 383 K.

Titration Experiments. The UV−vis and CD titration experiments were carried out as follows. Portions of a solution of chiral ligand in CH_2Cl_2 were added to the solution of **1** (3 mL) in CH_2Cl_2 (for concentrations of porphyrins, see footnote a in Table 2) in a quartz cell, and UV−vis and CD spectra were taken after each addition. The obtained spectra were corrected for the decrease in the bis(Zn porphyrin) concentration.

Determination of the Binding Parameters for the Bisporphyrin 1 Complexation. The present model for the supramolecular chirogenesis in **1** upon interaction with the tweezer-forming bidentate ligands involves two major equilibrium steps: first ligation (K_1), resulting in formation of the monoligated tweezer species **1·L**, and second ligation (K_2), yielding the bis-ligated *anti*-**1·L$_2$** species (Figure 1).

The analysis of the complexation isotherm in order to obtain equilibrium parameters of the two steps and CD amplitudes of the supramolecular chirogenesis in **1** is done as follows. The K_1 values were obtained separately from titration experiments at low concentration conditions and used as initial parameters for the second step of the above-mentioned total equilibrium. The final association constants (K_1 and K_2) and CD amplitudes (A_{calc}) were obtained as the optimized parameters by nonlinear least-squares curve fitting of the complexation-induced UV−

(9) (a) Kupce, E.; Boyd, J.; Campbell, *J. Magn. Reson. B* **1995**, *106*, 300. (b) Sai, T.; Takao, N.; Sugiura, M. *Magn. Reson. Chem*. **1992**, *30*, 1041. (c) Sugiura, M.; Vashchenko, A. V.; Kimura, A.; Fujiwara, H. *J. Chem. Soc., Perkin Trans. 2* **2000**, 1489. (d) Liu, M.; Farrant, R. D.; Lindon, J. C. *Magn. Reson. Chem*. **1992**, *30*, 173.

vis optical density and CD intensity changes at 292 K to the theoretical equations as described for the simpler two-step complexation model in our previous work.[4b]

The equilibrium parameters (K) and CD amplitudes (A_{calc}) of the supramolecular chirogenesis in **1** upon interaction with bidentate ligands, which do not form the tweezer structure were obtained according to the standard procedure described previously for monodentate ligands.[4b]

Definition of the H−H Distances by the Selective Relaxation Method. The procedure of the selective relaxation method is shown in Scheme 1, where the cross relaxation terms (σ_{ij}) were obtained from two kinds of relaxation time, nonselective T_1, T_1^{NS}, and selective noninversion T_1, T_1^{SNI}; the correlation time for the molecular reorientation (τ_c) was evaluated from the frequency dependence of T_1^{NS}. The interproton distances (r_{ij}) were then estimated by using these σ_{ij} and τ_c values.[9b,c]

In a multi-spin system, the nonselective T_1 of proton i, $T_1^{NS}(i)$, was formulated in the following equation

$$\frac{1}{T_1^{NS}(i)} = R^i(\text{all}) = \sum_j R^i(ij) = \sum_j N_j \sigma_{ij} + R^i(i) = \sum_j N_j \sigma_{ij} + \sum_j N_j \rho_{ij} + \rho^* \quad (1)$$

where R is the relaxation rate; R^i(all), $R^i(ij)$, and $R^i(i)$ are the relaxation rates of proton i under the conditions where all protons are inverted, only proton i and j are inverted, and only proton i is inverted, respectively; N_j is the number of magnetically equivalent nuclei for proton j; ρ_{ij} and σ_{ij} are the direct and the cross relaxation terms, respectively, for proton pair i and j; and ρ^* includes the relaxation terms other than intramolecular dipolar interactions. The selective noninversion relaxation time, T_1^{SNI}, was defined as the relaxation time observed under the condition in which all spin were inverted except one; and then the recovery to thermal equilibrium was monitored for all the spins inverted. Thus, it was formulated in the following equation[9d]

$$\frac{1}{T_1^{SNI}(i,j)} = R^i(\text{all}\neq j) = \sum_{k\neq j} R^i(ik) = \sum_{k\neq j} N_k \sigma_{ik} + R^i(i) = \sum_{k\neq j} N_k \sigma_{ik} + \sum_k N_k \rho_{ik} + \rho^* \quad (2)$$

where $T_1^{SNI}(ij)$ and $R^i(\text{all}\neq j)$ are the relaxation time and rate, respectively, of the proton i under the condition where all protons except j are inverted. Furthermore, ρ_{ij} and σ_{ij} were represented as in the following equations

$$\rho_{ij} = \frac{1}{10}\gamma^4 \hbar^2 r_{ij}^{-6}\left(\tau_c + \frac{3\tau_c}{1+\omega^2\tau_c^2} + \frac{6\tau_c}{1+4\omega^2\tau_c^2}\right) \quad (3)$$

$$\sigma_{ij} = \frac{1}{10}\gamma^4 \hbar^2 r_{ij}^{-6}\left(\frac{6\tau_c}{1+4\omega^2\tau_c^2} - \tau_c\right) \quad (4)$$

where γ is the proton gyromagnetic ratio, $\hbar$ is Planck's constant divided by 2π, r_{ij} is the interproton distance between protons i and j, ω is the Larmor precession frequency, and τ_c is the correlation time for molecular reorientation.

This analysis was based on the approximation that the system is a summation of two-spin contributions, which could be limited to the T_1 value obtained from the initial rate region of the relaxation exponential curve.[9b,c] On the basis of eqs 1 and 2, the cross-relaxation term, σ_{ij}, was expressed as the difference between the nonselective and selective relaxation rates resulting in the following equation

SCHEME 1

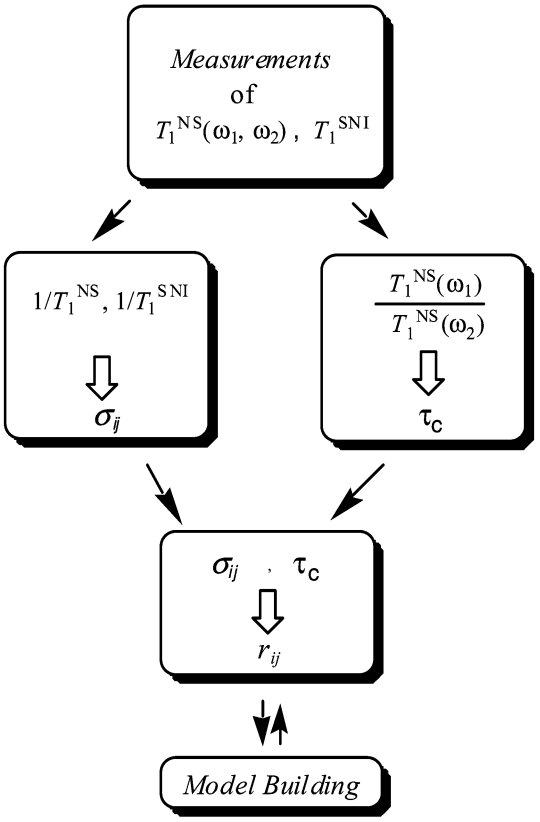

$$\frac{1}{T_1^{NS}(i)} - \frac{1}{T_1^{SNI}(i,j)} = R^i(\text{all}) - R^i(\text{all}\neq j) = N_j \sigma_{ij} \quad (5)$$

thus removing any contributions from nondipolar relaxation term such as paramagnetic oxygen or the quadrupolar effects of nitrogen. Finally, the interproton distance, r_{ij}, was estimated from the value of σ_{ij} (see eq 4), if a reasonable estimation was given for the value of τ_c. To estimate the τ_c value, the frequency dependence of the T_1^{NS} was used. If the condition $\rho^* \ll (\sigma_{ij} + \rho_{ij})$ is satisfied, upon substituting eqs 3 and 4 in eq 1 and taking the ratio of eq 1 at two frequencies and rearranging, τ_c for any proton was evaluated from a knowledge of the T_1^{NS} values at two different frequencies for a given proton according to the following equation:

$$\frac{T_1^{NS}(\omega_1)}{T_1^{NS}(\omega_2)} = \frac{(5+8\omega_2^2\tau_c^2)(1+5\omega_1^2\tau_c^2+4\omega_1^4\tau_c^4)}{(5+8\omega_1^2\tau_c^2)(1+5\omega_2^2\tau_c^2+4\omega_2^4\tau_c^4)} \quad (6)$$

Results and Discussion

1. Supramolecular Systems. Bis-porphyrin **1**,[2] which is connected by a short covalent ethane bridge (Figure 1), has been chosen as an achiral host molecule. As mentioned above, this compound is well-suited for the study of supramolecular chirogenesis upon interaction with monodentate guest molecules.[4] Essentially, for chirality induction purposes, only one binding center is necessary to ensure the steric repulsive interactions between the coordinated ligand and neighboring porphyrin ring, which are responsible for the asymmetry transfer mechanism, which has been proved by study of

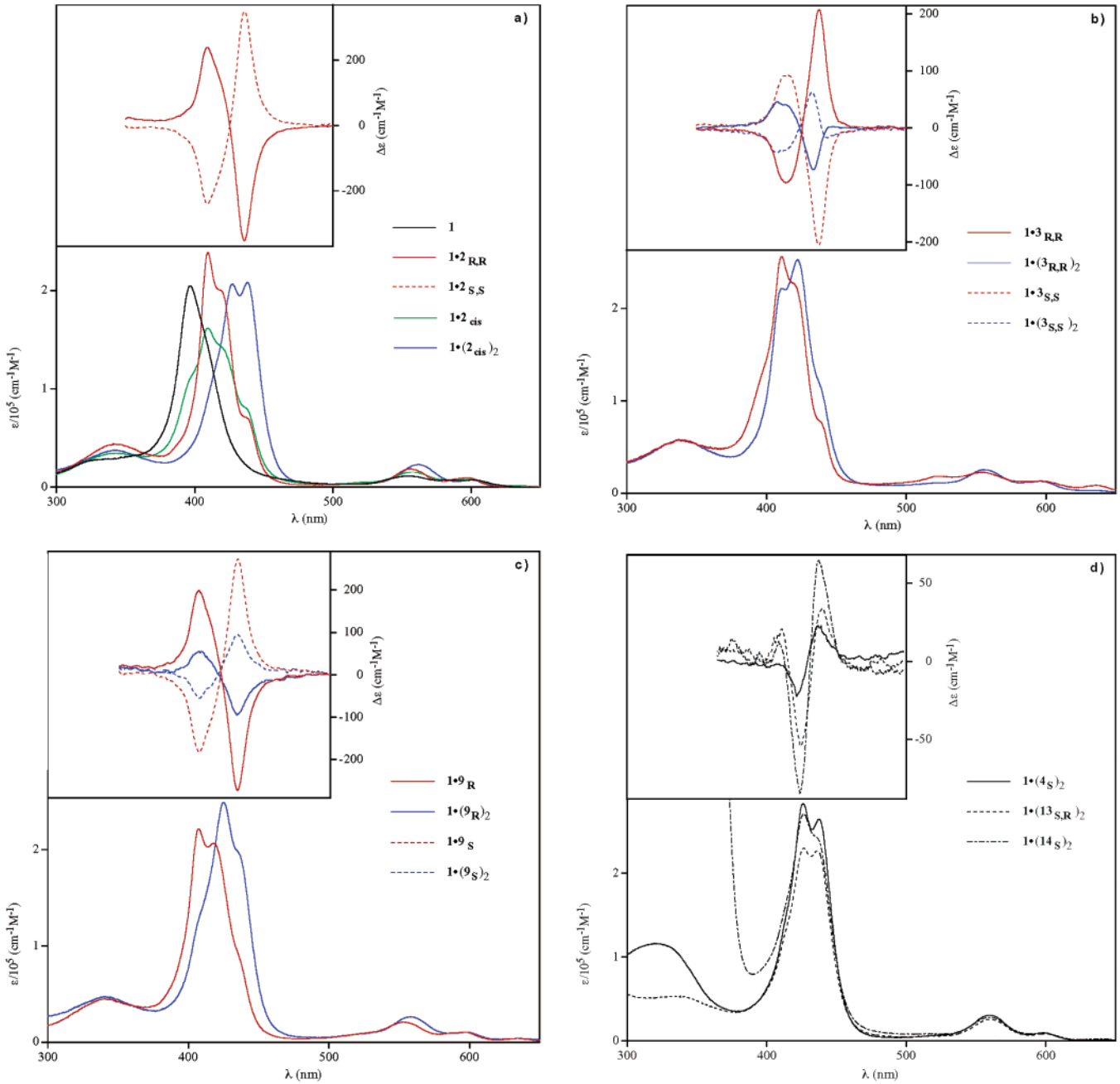

FIGURE 2. UV−vis and CD (inset) spectra of **1** in CH_2Cl_2 at 292 K without ligand and in the presence of different bidentate ligands (diamines and amino alcohols).

the corresponding monozinc derivative of bis-porphyrin.[10] However, the second metalated porphyrin ring in **1** besides its function as a repulsive counterpartner and/or chirality inducer may play a different role as the second binding site for bis- (or multi) functional compounds, thus resulting in a new type of structural organization and spectral properties. To investigate this possibility, several bidentate ligands **2**−**15** have been chosen as chiral guests (Figure 1). To ensure effective host−guest binding, all the ligands studied possess amino group(s) because of their well-known ability to coordinate to zinc porphyrins and form stable pentacoordinative adducts at room temperature.[11] These guests can be classified into several structurally analogous categories: (1) aliphatic, aromatic, and cyclic diamines **2**−**7**, (2) aliphatic amino alcohols **8**−**11**, and (3) aromatic amino alcohols **12**−**15**. While it is expected that both amino groups of diamines are able to interact with two binding sites in **1** to produce a stable 1:1 complex, of particular interest is the study of amino alcohols, with respect to their ability (or not) to form similar bis-coordinated structures, whereas besides the expected amino substituent binding, the normally room-temperature inert hy-

(10) Borovkov, V. V.; Hembury, G. A.; Yamamoto, N.; Inoue, Y. *J. Phys. Chem A*, in press.

(11) Smith, K. M. *Porphyrins and Metalloporphyrins*; Elsevier: Amsterdam, 1975.

droxyl group[3b,4b,e] may be also able to interact with the second zinc porphyrin ring.

Hence, to investigate interactions of the host **1** with bidentate guests **2**−**15** in detail several spectroscopic methods have been applied.

2. UV−vis Spectral Properties. In the beginning, the complexation behaviors of **1** and **2**−**15** were examined by absorption spectroscopy.

Upon interaction of **1** with bidentate ligands, two major spectral patterns were discovered in the UV−vis spectra, which differ drastically from the spectrum of the initial *syn*-**1** and are found to be dependent on the host−guest molar ratio and ligand's structure (Figure 2, Table 1). Notable features of the first spectral pattern are as follows. The porphyrin B (Soret) band is bathochromically shifted in comparison to that of the nonligated *syn*-**1** and exhibits three well-resolved transitions: at 407−411 nm as the main absorption peak, as well as absorption shoulders at 416−423 nm and 434−437 nm. The changes in the porphyrin Q-band region (500−700 nm) are less pronounced and essentially characterized by a marked enhancement of the Q_{01} transition intensity in comparison to the Q_{00} transition (in *syn*-**1,** the intensities of Q_{00} and Q_{01} bands are almost the same). A high-energy transition (around 340 nm) associated with ligand coordination to metalloporphyrins is also observed in the first spectral pattern. This type of spectrum is observable in the low ligand molar excess region upon addition of **2**, **3**, **5**−**12**, and **15**.

The second observed spectral pattern is characterized by a further low energy shift and splitting of the Soret band into two well-resolved transitions in the region of 423−438 nm, and additional enhancement of the Q_{01} band intensity over the Q_{00} transition. This UV−vis profile is well-known and typical for the extended *anti*-**1**·$\mathbf{L}_2$ species that has been previously described in detail.[4] Therefore, as expected, all guests studied (excepting $\mathbf{2_{R,R}}$ and $\mathbf{2_{S,S}}$) lead to this second spectral pattern at high ligand molar excess, while in the cases of **4**, **13**, and **14** this spectral profile is observed even at low ligand molar excess. Since the second spectral pattern is associated with the 1:2 host−guest complexation, it is reasonable to suggest that the first spectral pattern is induced by the 1:1 host−guest complex **1**·**L** (comprehensive proofs of this are presented in the following text).

Examination of CPK molecular models reveals that the majority of bidentate ligands studied can readily enter and be accommodated between the two porphyrin planes of the bis-porphyrin, yielding a 1:1 tweezer complex **1**·**L**, which is stabilized synergetically by two spatially well-orientated Zn−N (and/or Zn−O) coordination bonds (Figure 3).

According to Kasha's exciton coupling theory,[12] while two coupling electronic transitions are moving away from the parallel dipoles' orientation toward the in-line dipoles' orientation, the oscillator strength of the low energy component in the absorption spectrum is enhanced. Upon ligation and subsequent switching of the porphyrin conformation from the syn form into the tweezer form, the orientation of porphyrin B electronic transitions is

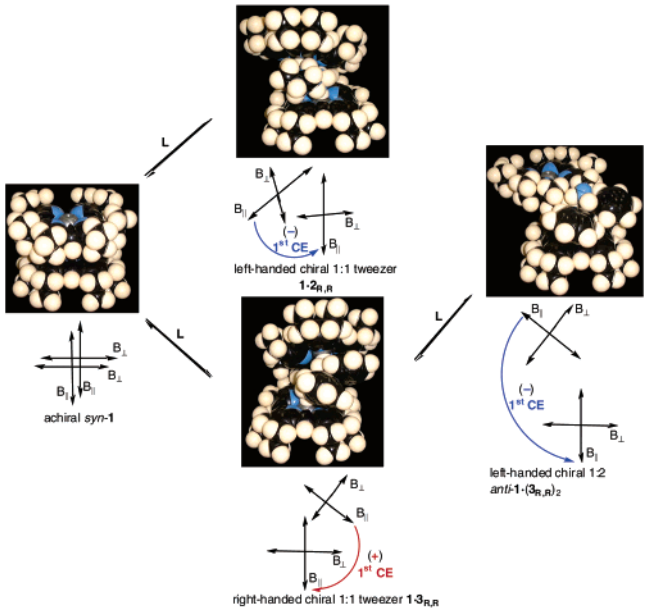

FIGURE 3. Mechanism of supramolecular chirogenesis in **1** by bidentate chiral guests ($\mathbf{2_{R,R}}$ and $\mathbf{3_{R,R}}$): CPK molecular models and corresponding coupling electronic transitions.

also changed from the initial parallel alignment,[13] thus increasing the probability of the bathochromically shifted absorption bands in the UV−vis spectra that were observed experimentally as two shoulders of the low energy side of the Soret band (Figure 2, Table 1).[14] As the second ligation step takes place leading to the formation of the anti conformation, the porphyrin B transitions (particularly, the lowest energy $B_{||}$ transitions) are aligned in a more in-line fashion resulting in further enhancement of the bathochromically shifted absorption bands, thus yielding the well-known split pattern of the Soret band of the *anti*-**1**·$\mathbf{L}_2$ species.[4]

As mentioned above, the UV−vis spectral changes are strongly dependent upon the structure of bidentate ligands. All the diamines studied, except **4**, are able to form the 1:1 tweezer complex **1**·**L**. This is a result of the high binding affinity of the NH_2 groups for the Zn central ions, when accommodated between the two porphyrin rings, as seen in 1,2-substituted diamines **2** and **3**, *terminus* diamines with a flexible covalent linkage **5**, and five-membered rings such as the imidazoles **6** and **7**. It is interesting to note that in the case of the six-membered ring **4**, its rigidity and large interamine distance result in an unfavorable geometry which prevents it entering the interporphyrin cavity to form a tweezer structure, thus producing only the standard 1:2 anti structure. As also expected, the majority of diamines generate the anti structure at high concentrations via shifting the total complexation equilibrium (Figure 1). However, the most

(12) Kasha, M.; Rawls, H. R.; El-Bayoumi, M. A. *Pure Appl. Chem.* **1965**, *11*, 371.

(13) The syn structure in Figure 3 is schematically shown in a strictly parallel orientation, while in reality it is a racemic mixture of the right- and left-handed slipped conformations.

(14) The main absorption peak of **1**·**L** at 407−412 nm is apparently due to the dominant close-to-parallel orientation of the B transitions in the tweezer conformation. The observed bathochromic shift of this peak (in comparison to the absorption of *syn*-**1**) is caused by the ligation, as also seen in the case of the formation of the corresponding μ-oxo species of bis(iron porphyrin), which exists in a similar tweezer form. (Hembury, G. A.; Borovkov, V. V.; Lintuluoto, J. M.; Inoue, Y. *Chem. Lett.* **2003**, *32*, 428−429.)

surprising results were obtained in the case of enantiopure $\mathbf{2_{R,R}}$ and $\mathbf{2_{S,S}}$. These ligands form the 1:1 tweezer complex **1·L** exclusively, regardless of the amount of ligand added, while their achiral analogue $\mathbf{2_{cis}}$ follows the general tendency of the two-step equilibrium (syn-tweezer-anti). This extraordinary stability of the tweezer structure in $\mathbf{2_{R,R}}$ and $\mathbf{2_{S,S}}$ arises from two strong coordination bonds made by the two preorganized amino groups, which are oppositely orientated above and below the plane of the cyclohexane ring, and lack of bulky substituents that may generate steric repulsions leading to disruption of the tweezer structure. However, in the case of $\mathbf{2_{cis}}$, the two amino groups are located on the same side of the cyclohexane ring, thus producing an unfavorable geometry for the tweezer formation and accordingly decreasing the stability of the 1:1 complex. Furthermore, the attractive CH$-\pi$ interactions between the ligand (for $\mathbf{2_{R,R}}$ and $\mathbf{2_{S,S}}$) and porphyrin may additionally contribute to the stability of the tweezer complex. Similar behavior of binding strength enhancement was also observed for a monodentate ligands containing the cyclohexyl fragment upon interaction with zinc porphyrins.[4b] The positive role of this factor in the supramolecular association processes has been previously confirmed and thoroughly investigated.[15]

In the case of aliphatic amino alcohols, the ligands produce both supramolecular species: the 1:1 tweezer and 1:2 anti structures at low and high ligand concentration, correspondingly. It is important to note that formation of the tweezer structure implies that the hydroxyl group is able to bind to the second zinc porphyrin in the bis-porphyrin host. In general, monodentate alcohol ligands are known to have only a weak affinity for zinc porphyrins, exhibiting positive free energy changes for the complexation processes at room temperature.[3b,4b] Apparently, the first binding step of the amino group enhances the second binding of the hydroxyl group via structural preorganization of the bis-porphyrin host, thus making the latter thermodynamically favorable. However, increasing the substituent's bulkiness by introducing aromatic groups results in a decreasing of the hydroxyl binding. Thus, while the first phenyl group at the chiral center or remote position in **12** and **15**, respectively, does not hinder formation of the tweezer structure, the second phenyl group attached at the neighboring or the same carbon in **13** and **14**, respectively, results in drastic switching of the direction of the association process yielding the anti structure exclusively without formation of the tweezer complex. This is apparently caused by excessive steric bulkiness around the binding sites that competes successfully with the binding of the second functional (OH) group.

3. CD Spectral Properties and Mechanism of Supramolecular Chirality Induction. Simultaneous (with UV−vis)CD monitoring of the complexation process between bis-porphyrin **1** and chiral bidentate ligands reveals the appearance of optical activity in the porphyrin Soret band region due to effective asymmetry transfer from chiral guests to achiral host (Figure 2, insets and Table 1).[16] As found in the case of UV−vis spectroscopy, in the CD spectra of the tweezer forming systems there are two different spectral patterns at low and high ligand concentrations which are associated with the tweezer **1·L** and anti-$\mathbf{1{\cdot}L_2}$ complexes, respectively. The CD spectral profile of **1·L** (Figure 2a−c, insets) consists of complex bisignate and non equivalent Cotton effects of high intensities due to superposition of the optically active eight allowed transitions originated from the two corresponding pairs of porphyrin $B_{\parallel}$ and $B_{\perp}$ electronic transitions. Although all the allowed transitions have not yet been fully assigned, the good match between the position of the first Cotton effect (432−438 nm) and the most bathochromically shifted absorption band in the UV−vis spectrum, arising from the coupled lowest energy $B_{\parallel}$ transitions, implies the same origin of these transition. The asymmetrical shape and considerable broadening of the second Cotton effect is also a clear indication of the contribution of several higher energy transitions of opposite signs. Further addition of the bidentate ligands results in drastic transformations in the CD spectra, involving reduction of the signal amplitude and appearance of the well-established spectral profile corresponding to the *anti*-$\mathbf{1{\cdot}L_2}$ species. A similar type of CD spectrum, as expected, is also observed in the cases of the chiral bidentate ligands **4**, **13**, and **14**, which induce the anti structure only.

Upon analyzing CPK molecular models, it was found that the chirality transfer mechanism in **1·L** is based upon chiral deformations in the host molecule arising from the adoption of a screw structure by the bis-porphyrin upon accommodation of a bidentate ligand between the two porphyrin planes, following the guest's geometry and minimizing the steric hindrances (Figure 3). As this takes place, coupling of the porphyrin electronic transitions occurs in a stereospecific manner, thus inducing the optical activity in the region of the porphyrin absorption. The intensity of induced CD couplet depends on stability and geometry of the tweezer complex, while the chirality sign is governed by the coupling direction of the lowest energy electronic transitions. According to the exciton chirality method,[17] a clockwise orientation of two through-space-interacting electric dipoles produces positive chirality, while an anticlockwise orientation leads to negative chirality, corresponding to positive and negative signs of the first Cotton effect derived from the exciton coupling. The spatial orientation of the two porphyrin rings in **1·L** is essentially dependent upon the pre-organization of the ligand's functional groups and the steric interactions between host and guest molecules. The combination of these factors results in the majority of bidentate ligands with *R* absolute configuration inducing a left-handed twist, while (*S*)-ligands produce a right-handed twist. The lowest energy $B_{\parallel}$ coupling porphyrin transitions are orientated in an anticlockwise fashion in

(15) (a) Mizutani, T.; Wada, K.; Kitagawa, S. *J. Am. Chem. Soc.* **1999**, *121*, 11425. (b) Kobayashi, K.; Asakawa, Y.; Kikuchi, Y.; Toi, H.; Aoyama, Y. *J. Am. Chem. Soc.* **1993**, *115*, 2648.

(16) Because of the multi equilibrium character of the complexation process, while the position of CD bands can be determined precisely on the wavelength scale, the signals' intensities and the total CD amplitude (A_{obs}) of the tweezer complexes (with exception of $\mathbf{2_{R,\,R}}$ and $\mathbf{2_{S,\,S}}$) can be estimated only with some degree of uncertainty due to contributions of the chiral anti structure (more precise data obtained by optimization of the titration curves will be discussed in Chapter 3). Also the A_{obs} values of the *anti*-$\mathbf{1{\cdot}L_2}$ species are not discussed in this chapter due to the same reason.

(17) Harada, N.; Nakanishi, K. *Circular Dichroic Spectroscopy. Exciton Coupling in Organic Stereochemistry*; University Science Books: Mill Valley, CA, 1983.

the left-handed structure and in a clockwise fashion in the right-handed structure, which correspond to the negative and positive chirality observed experimentally (Figure 2 and Table 1). However, in contrast to the simple bulkiness factors playing the key role in the chirogenesis processes observed in the anti complexes formed by monodentate ligands,[4c−f] in the case of bidentate guests the orientation of the binding groups in the tweezer complexes is primarily responsible for the helical sense of the screw. Therefore, a different binding group orientation may result in inversion of the twist direction and subsequent induction of opposite chirality. Indeed, among the ligands studied there are a few exceptional guests **3**, **10**, and **11**, which give rise to chirality opposite to that observed in all other tweezer complexes.[18] Apparently, the minimization of the steric hindrances in the **1·L** complexes is the prime reason for such spatial inversion of the functional groups in these ligands. For example, a CPK model of $\mathbf{1{\cdot}3_{R,R}}$ clearly shows that the folded conformation of this ligand results in minimal host−guest steric clashes (Figure 3). In this conformation, the orientation of two amino groups is exactly opposite to that of other "regular" ligands, such as $\mathbf{1{\cdot}2_{R,R}}$.

As mentioned above, another parameter of the supramolecular chirogenesis is the intensity of the induced CD signal, which is dependent upon conformational freedom of the complex to form the right- and left-handed screw structures, as well as distance and dihedral angle between the coupling electronic transitions. In the cases of the 1,2-substitued ligands **2**, **8**, **9**, **12**, and **15** it is their similar geometries that result in tweezer structures of the same chirality. Remarkably, and due to the complexes stability arising from the aforementioned pre-organization, the tweezer complexes $\mathbf{1{\cdot}2_{R,R}}$ and $\mathbf{1{\cdot}2_{S,S}}$ form essentially unidirectional screws, generating the greatest degree of chirality induction ever reported for this bis-porphyrin host in solution.[4b−f] Other analogous ligands **8**, **9**, **12**, and **15** give the smaller A_{obs} values (Table 1), apparently as a result of the presence of tweezer complexes of the opposite screw sense due to the flexibility of the ligand and the lesser binding affinity of the amino alcohol guests (see Chapter 3). It is important to note that the ligand $\mathbf{5_S}$ with a flexible hydrocarbon chain between two amine groups and the imidazole containing $\mathbf{6_S}$ generate considerable CD signals with A_{obs} values close to those observed in the case of enantiopure **2**. This indicates that the two porphyrin rings in $\mathbf{1{\cdot}5_S}$ and $\mathbf{1{\cdot}6_S}$ have a similar spatial arrangement to that found in the case of the tweezer complexes formed by the rigid cyclic ligands **2**, owing to strong binding of the two amino groups and regardless of the number of the chiral centers and the structure of a covalent tether between the amino groups. Besides binding factors, differences in the chiral steric field experienced by the two porphyrin moieties, as a result of variations in the relative bulkiness around each binding site of the complexed ligand, substantially affects the chirogenesis process in **1·L**. In particular, elongation of the side chain in **9** in comparison to **8** results in marked enhancement of the ligand's substituent size disparity, thus increasinging the CD amplitude. Another example is seen in the case of the **10**/**11** pair where replacement of the methyl group with a hydrogen substituent also increases the distinction between the substituents, thus again resulting in increased chirality.

As mentioned in Chapter 1, further increase of the ligand concentration (for the tweezer forming ligands, except $\mathbf{1{\cdot}2_{R,R}}$ and $\mathbf{1{\cdot}2_{S,S}}$) shifts the total equilibrium to the *anti*-$\mathbf{1{\cdot}L_2}$ species, which was explicitly shown by UV−vis spectroscopy. In the case of CD spectroscopy, although quantitative analysis of this process is not discussed in this chapter,[16] qualitatively, there are clear tendencies of decreasing induced CD amplitudes and the transformation of the signal profiles (Figure 2b,c, insets) to that already well-known for the anti species.[4] The chirality sign of the newly formed *anti*-$\mathbf{1{\cdot}L_2}$ is in full agreement with the previously established principles of the bulkiness−priority rule relationships for supramolecular chirality induction by monodentate ligands (see the Introduction). Hence, when the substituent's bulkiness order at the asymmetric carbon coincides with the priority rule, bidentate ligands with the *R* absolute configuration at the chiral center closest to the amino binding group induce negative chirality due to anticlockwise orientation of the lowest energy B_{II} coupling porphyrin transitions in *anti*-$\mathbf{1{\cdot}L_2}$ (Figure 3), while in the case of (*S*)-ligands the situation is exactly opposite resulting in positive chirality.[19] As this equilibrium shift occurs, an intriguing phenomenon of chirality inversion is observed for bidentate ligands **3** and **10**, which have "irregular" signs of their tweezer complexes. Remarkably, this takes place in a pure two-component molecular assembly consisting of only an achiral host and a chiral guest and is controlled solely by its stoichiometry, which is a rarely observed physicochemical process.[20] In the case of ligands **4**, **13**, and **14**, which do not form the tweezer complex, their *anti*-$\mathbf{1{\cdot}L_2}$ complexes exhibit the chirality signs according to general tendencies observed for monodentate ligands,[4] which are described above.

To investigate the detailed binding mechanism of supramolecular chirogenesis in **1** upon interaction with bidentate ligands and obtain the corresponding equilibrium parameters, titration experiments using optical spectral methods have been carried out.

4. Supramolecular Equilibria and Mechanism of Guest Binding to the Bis-porphyrin Host 1. Taking into account the qualitative changes in the UV−vis and CD spectra of **1** upon interaction with bidentate ligands described in previous chapters, the corresponding binding and spectral parameters were obtained by UV−vis and CD titration experiments carried out at the low and high ligand molar excesses, and the complexation mechanism thoroughly examined.

4.1. UV−vis and CD Spectral Changes. Stepwise addition of bidentate ligands to **1** produces dramatic

(18) Although this discrepancy hinders application of the tweezer structure for the chirality diagnosis purposes in the case of some bidentate ligands, there are two effective solutions for overcoming this problem, which include (1) further increase of the ligand concentration to shift the equilibrium towards the anti structure, thus inducing the "right" sign of CD signal (see discussion below); and (2) use of a new chirality sensor on the basis of monometalated bis-porphyrin[10] that never produces the tweezer conformation and always yields the anti conformation with the correct sign of CD signal.

(19) The negative chirality induced by $\mathbf{11_S}$ is apparently a result of a discordance between the bulkiness order and priority rules as previously observed for several amino acid derivatives (see ref 4d).

(20) There is another example of the stoichiometry effect reported for a certain tetrapyrrole host; see: Edinger, J.; Falk, H.; Jungwirth, W.; Müller, N.; Zrunek, U. *Monatsh. Chem.* **1984**, *115*, 1081.

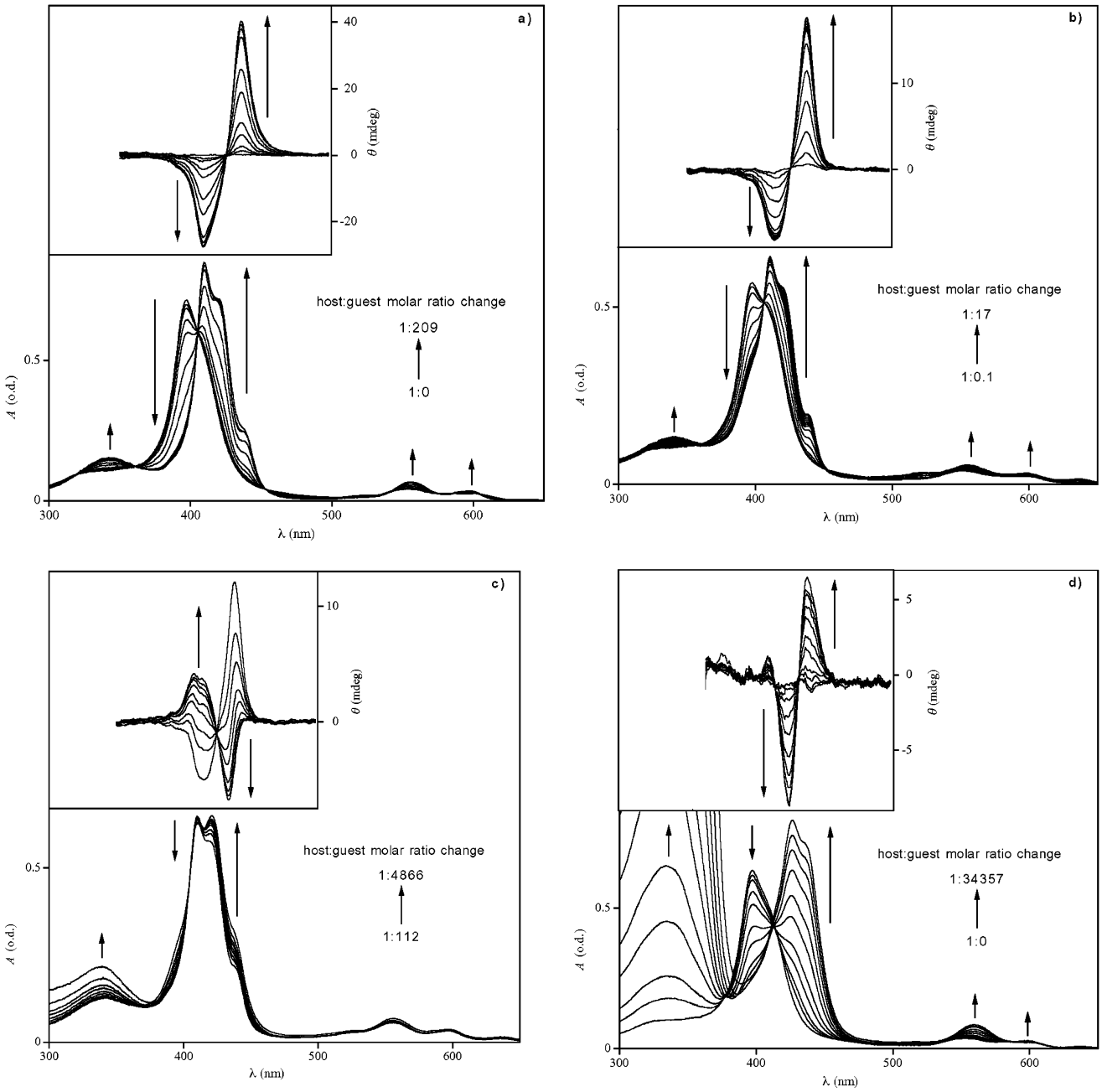

FIGURE 4. UV−vis and CD (insets) spectral changes of **1** upon addition of $\mathbf{2_{S,S}}$ as the host:guest molar ratio changes from 1:0 to 1:209 (a), $\mathbf{3_{R,R}}$ as the host/guest molar ratio changes from 1:0.1 to 1:17 (b), $\mathbf{3_{R,R}}$ as the host/guest molar ratio changes from 1:112 to 1:4870 (c), $\mathbf{14_S}$ as the host/guest molar ratio changes from 1:0 to 1:34360 (d).

transformations in the UV−vis and CD spectra. As stated above, there are two distinct concentration regions found in the supramolecular chirogenesis process corresponding to formation of the tweezer **1·L** and *anti*-$\mathbf{1·L_2}$ species. The representative spectral changes are shown in Figures 4a-*d*. In the UV−vis spectra of the tweezer formation (Figures 4a,b) the intensity of the B band at 397 nm progressively decreases upon increase of the ligand molar excess from 1:0 to 1:209 or 1:17 (in the case of $\mathbf{2_{S,S}}$ and $\mathbf{3_{R,R}}$, correspondingly) and a new spectral pattern of the tweezer **1·L** species, which was characterized in detail in Chapter 2, appears. Upon formation of the *anti*-$\mathbf{1·L_2}$ species by further increase of the host:guest molar ratio from 1:112 to 1:4870 for the tweezer inducing $\mathbf{3_{R,R}}$ or from 1:0 to 1:34360 for $\mathbf{14_S}$ (which does not form the tweezer), the changes include diminishing the spectral pattern of the **1·L** structure (for $\mathbf{3_{R,R}}$) and the appearance and enhancement of the typical transitions associated with the *anti*-$\mathbf{1·L_2}$ species (for $\mathbf{3_{R,R}}$ and $\mathbf{14_S}$) (Figure 4c,d) that were also described in Chapter 2 and reported previously.[4] However, as a result of the high stability of the tweezer complex even at large excesses of $\mathbf{3_{R,R}}$ complete conversion to the 1:2 complex is not achieved, while compound **2** does not form the *anti*-$\mathbf{1·L_2}$ species as previously discussed.

In the CD spectra induced by $\mathbf{2_{S,S}}$ and $\mathbf{3_{R,R}}$ there is the appearance of a bisignate CD signal consisting of two major Cotton effects of opposite sign that gradually

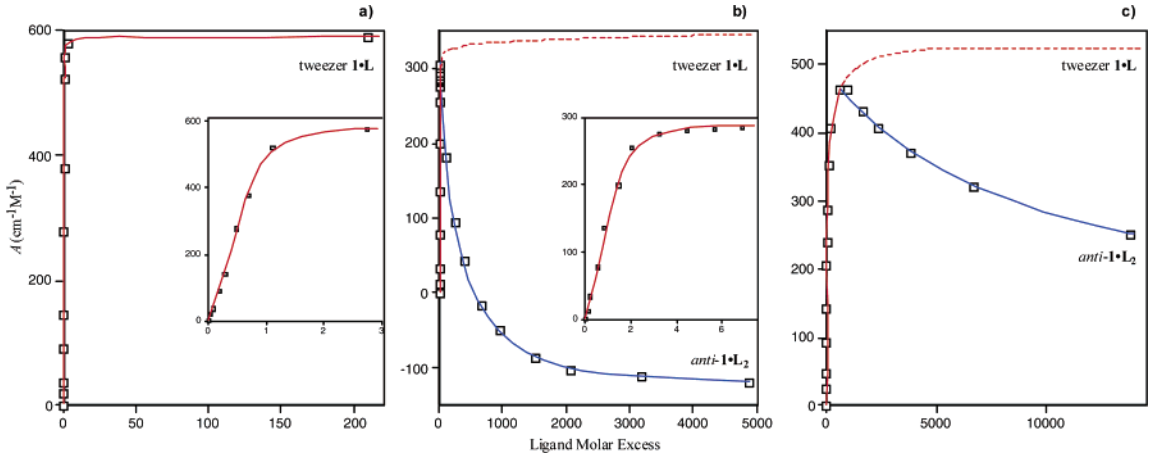

FIGURE 5. Dependence of the CD amplitude of **1** upon the molar excess of $\mathbf{2_{S,S}}$ (a), $\mathbf{3_{R,R}}$ (b), and $\mathbf{9_S}$ (c). The solid red and blue lines represent the best theoretical fits for the 1:1 and 1:2 host−guest complexation processes, respectively (see the Experimental Section). Insets: expanded area of the CD amplitude dependence at the low ligand molar excess region.

enhance as the ligand concentration increases due to formation of the **1·L** species (Figure 4a,b, insets). The spectral profile and various factors controlling the intensities and sign of the induced couplet were discussed in Chapter 3. In the case of $\mathbf{2_{S,S}}$ the spectral changes are unidirectional exhibiting a saturation behavior at high ligand concentrations (Figure 4a, inset). However, further addition of $\mathbf{3_{R,R}}$ causes drastic CD spectral transformations due to a stepwise equilibrium shift toward the *anti*-$\mathbf{1·L_2}$ complex (Figures 4c, inset), which include reduction of the CD amplitude followed by chirality inversion with a positive CD couplet gradually transforming into a new negative CD couplet. While the former is a general tendency for other bidentate ligands involving in the two-step equilibrium, the latter is an "exceptional" event observed for **3** and **10** only, as described above. Bulky $\mathbf{14_S}$ shows the appearance and gradual enhancement of the well-known bisignate CD signal corresponding to the *anti*-$\mathbf{1·L_2}$ species (Figure 4d, inset).

4.2. Definition of the Binding Parameters. The UV−vis changes are followed at wavelengths corresponding to the maximum of the most intense B transition of the tweezer **1·L** species, and as in the case of monodentate ligands,[4b] at the maximum of the more bathochromically shifted B_{II} transition of the *anti*-$\mathbf{1·L_2}$ species, to analyze the first and second equilibrium steps, respectively. The latter is also used for the ligands forming the *anti*-$\mathbf{1·L_2}$ complexes only. For CD spectroscopy the total CD amplitude is chosen as a monitoring parameter. These particular spectral parameters are selected due to the same advantages as reported previously.[4b] Representative plots of the UV−vis and CD monitoring data versus the molar ligand excess are shown in Figures 5 and Figure S2 (Supporting Information). There is a good coincidence of the UV−vis and CD experimental points indicating at the same origin of these spectral changes. In contrast to monodentate ligands, bidentate ligands, which generate the tweezer structure (with the exception of $\mathbf{2_{R,R}}$ and $\mathbf{2_{S,S}}$), exhibit two distinct regions of the spectral data at low and high ligand molar excesses. Another profound difference between mono- and bidentate guests is that neither of these two regions shows a sigmoidal profile (typical for monodentate ligands) but rather a combination of two simple dependencies for each region, which were also observed for the monomeric zinc octaethylporphyrin (ZnOEP) upon interaction with monoamines.[4b] Interestingly, the CD plots at low guest concentrations exhibit a steep ascending behavior, while the plots at high concentrations show shallower descending profiles reflecting the differences in the binding strengths of the two species, while the higher CD intensity maximum of the tweezer, compared to the *anti*-$\mathbf{1·L_2}$ species, reflects its higher chirogenic properties. Furthermore, in the case of $\mathbf{3_{R,R}}$ the experimental points even change the sign from positive to negative due to the chirality inversion process, thus passing through the zero values at a host/guest ratio of ca. 1:550 (Figure 5b).

The experimental points at low and high ligand concentration regions are well-fitted to the set of theoretical equations for the two-step complexation model using nonlinear least-squares optimization (see the Experimental Section). This model contains two major steps for the total equilibrium shown in Figure 1:[21] the first ligation (K_1) resulting in incorporation of the ligand between the two porphyrin rings thus yielding the tweezer **1·L** and the subsequent second ligation (K_2) inducing conformational switching to give the *anti*-$\mathbf{1·L_2}$ species. The optimization allows determination of the K_1 and K_2 values as well as the calculated CD amplitudes (A_{calc}) for the **1·L** and *anti*-$\mathbf{1·L_2}$ complexes, which are listed in Table 2. As one can see, the general tendencies of supramolecular chirogenesis upon interaction between **1** and the tweezer-forming bidentate ligands are as follows. The K_1 values are significantly larger than the K_2 values reflecting the remarkable stability of the tweezer **1·L** structure over the *anti*-$\mathbf{1·L_2}$ form due to the optimal geometry and enhanced rigidity of the 1:1 complex as discussed above. In the case of the enantiomers of **2** and **3**, the first binding is exceptionally strong with the K_1 values exceeding 10^7 M^{-1}. Diamines have

(21) Although interaction of **1** with bidentate ligands is apparently a multistep equilibrium process containing different types of syn, anti and tweezer structures of various stoichiometries, a very good correlation of the experimental data with the theoretical two-step binding complexation allows the major equilibrium species shown in Figure 1 to be used for the plausible description of the supramolecular chirogenesis. Furthermore, all these species are stable enough to be detected and characterized individually by means of various spectroscopic techniques.

substantially larger corresponding K_1 and K_2 values than amino alcohols due to their greater affinity for zinc porphyrins. It is also important to note that besides binding affinity the ligand preorganization plays a key role in the complexation process, which can be perfectly illustrated with the difference between binding properties of chiral $\mathbf{2_{R,R}}$ and $\mathbf{2_{S,S}}$ on one hand and $\mathbf{2_{cis}}$ on the other hand. Thus, two oppositely orientated amino groups in $\mathbf{2_{R,R}}$ and $\mathbf{2_{S,S}}$ result in exclusive formation of the tweezer structure with $K_1 = 1.25 \times 10^7\ M^{-1}$, while location of the amino groups on the same side of cyclohexyl ring in $\mathbf{2_{cis}}$ considerably reduces the K_1 value by 1000 times and allows the second equilibrium step to the anti structure formation to take place. Additionally, as expected, steric hindrance is a negative factor in generation of the tweezer, as demonstrated by poorer binding affinity of bulkier monophenyl substituted amino alcohols **12** in comparison to those of less bulky aliphatic amino alcohols **8** and **9**. Upon introduction of an additional phenyl group in the case of diphenyl derivatives **13** and **14**, the enhanced crowding around the binding site completely blocks the formation of tweezer structure altogether.

Besides the above-mentioned optimization procedure, a Job's plot was obtained in order to confirm unambiguously the 1:1 stoichiometry of the tweezer complex **1·L** at low concentrations of bidentate ligands. Thus, a plot of the Soret band intensity changes (ΔA) at 411 nm against [**1**]/([**1**] + [$\mathbf{3_{R,R}}$]) has a minimum at 0.5 that corresponds to formation of the 1:1 complex at the low ligand molar excess region (see Figure S3, Supporting Information).

In the case of other bidentate ligands which do not form the tweezer structure, since their complexation behavior is the same as that of monoamines the equilibrium parameters are determined according to the previously reported method[4b] and listed in Table 2. The binding constants (K) of **4**, **13**, and **14** correlate with those of monodentate ligands[4b] and reflect their structural peculiarities. For example, the K value of **4** is larger than that of other similar ligands apparently due to the enhancement of complexation affinity caused by two amino binding groups in one guest molecule. In contrast, the K values of **13** and **14** are noticeably smaller in comparison to those of primary monoamines because of their excessive bulkiness, which may prevent facile access of these ligands to the porphyrin binding site. The weaker binding of bulkier **14** in comparison with **13** additionally supports this conclusion.

The energetics of the supramolecular chirogenesis is evaluated on the basis of the changes in the overall Gibbs free energy change ($\Delta G°$), which are calculated and listed in Table 2. The $\Delta G°$ values are substantially negative for all the systems studied indicating that the association processes are highly energetically favorable. However, diamine binding is more favorable in comparison to amino alcohols regardless of the operating complexation mechanism, reflecting the obvious energy gain due to ligation of two amino groups. The $\Delta G°$ values are also dependent upon the number of the equilibrium steps (two step complexation in the case of $\mathbf{2_{cis}}$ and **3** is more energetically favorable than one step complexation in the case of $\mathbf{2_{R,R}}$ and $\mathbf{2_{S,S}}$) and structure of the ligands (less crowded **8**, **9**, and **13** are more favorable than the corresponding **12** and **14**).

In addition to the binding and energetic parameters, the theoretical treatment of the titration experimental data (see the Experimental Section) allows the determination of spectral parameters such as the calculated CD amplitudes (A_{calc}) (see Table 2). This is particularly beneficial for multistep complexation processes when some equilibrium species cannot be obtained in a pure form and subsequently characterized, especially in the cases of the tweezer complexes induced by amino alcohols and the anti structures generated by tweezer forming bidentate ligands. Analyzing the resulting data, it is apparent that the A_{calc} values of **1·L** are larger than those of anti-$\mathbf{1{\cdot}L_2}$ due to the stability and geometrical reasons as discussed above. It is also noteworthy that the A_{calc} and A_{obs} values for **1·2** are essentially the same, a situation also found for **1·3**, thus indicating that the 1:1 tweezer complex can be obtained in an almost pure form experimentally — which is important for further characterization of the tweezer structure by different spectroscopic methods (see subsequent chapters). Interestingly, the A_{calc} values of tweezer complexes, which do not exhibit chirality inversion, are in the range of $\pm 465-589\ M^{-1}\ cm^{-1}$ and are practically independent of the ligand structure as a result of the similar spatial architecture of these systems. In sharp contrast to the tweezers **1·L**, chirality induction in *anti*-$\mathbf{1{\cdot}L_2}$ is strongly dependent upon various structural factors and follows the general rules previously discovered for monodentate guests.[4] Besides the ligand affinity, the major factors controlling supramolecular chirogenesis in *anti*-$\mathbf{1{\cdot}L_2}$ are difference in bulkiness between the substituents at the asymmetric carbon and position of the chiral center in relation to the binding group. Thus, for the same structural analogues, the A_{calc} values of *anti*-$\mathbf{1{\cdot}(12)_2}$ are greater than those of *anti*-$\mathbf{1{\cdot}(9)_2}$ because the Ph group of **12** is larger than the *i*-Bu substituent of **9**, while in the case of *anti*-$\mathbf{1{\cdot}(3)_2}$ and *anti*-$\mathbf{1{\cdot}(13)_2}$ the A_{calc} values are essentially the same owing to the nearly identical substituents at the chiral center. The *anti*-$\mathbf{1{\cdot}(4)_2}$ and *anti*-$\mathbf{1{\cdot}(8)_2}$ complexes possess small or almost no optical activity due to location of the asymmetric carbon at the β-position with respect to the binding site[22] as was previously observed for monodentate ligands. Furthermore, for **8** there is an additional factor diminishing the chirogenic properties which is the marginal difference in bulkiness between the OH and Me groups.

Thus, the above spectral analysis allows discovery and identification of the new highly optically active tweezer structure, which is a key element in the supramolecular chirogenesis induced in **1** upon interaction with the majority of bidentate ligands. The ensuing chapters discuss further investigation of these new **1·L** species by other relevant spectroscopic methods. For this purpose enantiopure **2** (and **3** in the case of ESI MS) are chosen as the corresponding ligands for generation of **1·L** owing to their unique ability to form the tweezer structure exclusively.

5. Q Band Region: Absorption and Fluorescence Spectral Properties. As stated in Chapter 2, besides highly intense B bands (as extensively discussed above),

(22) In the case of **4** it is most likely that the least sterically hindered nitrogen predominantly binds to the zinc porphyrins forming *anti*-$\mathbf{1{\cdot}L_2}$, which results in β-location of the chiral center.

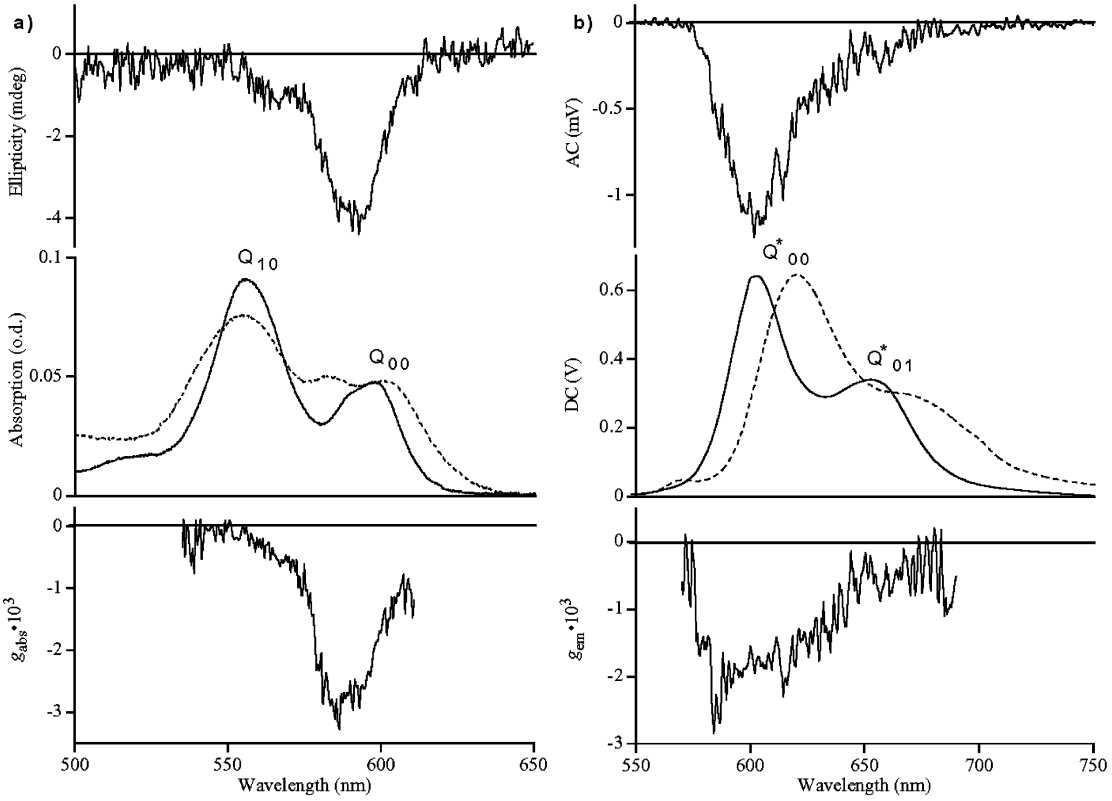

FIGURE 6. CD and UV−vis spectra (Q-band region) with the corresponding absorption anisotropy (g_{abs}) factors (a) and CPF and fluorescence spectra with the corresponding fluorescence anisotropy (g_{em}) factors (b) of **1·2$_{R,R}$** (solid lines) and **1** (dashed lines) in CH_2Cl_2. The UV−vis and fluorescence spectra were normalized to the same intensity of the corresponding 0−0 transitions.

porphyrin chromophores also exhibit absorption to the singlet excited state in the visible spectral region that corresponds to the low energy quasi-allowed Q transitions. Despite the decreased intensity, these bands are crucial for characterization of the porphyrin structure, coordination, conformation, photophysics and particularly fluorescence properties. In the case of chirogenic phenomena, investigation of the Q transitions may provide an additional insight into the optical activity not only during the light absorption events but also during the light emission processes. However, among a substantial number of references devoted to the chirality induction in porphyrins, there are very few examples of the CD spectra of the Q-bands[1d,23] and, to our knowledge, none of the CPF spectra. These shortcomings are usually caused by a low efficiency of the asymmetry transfer processes resulting in only small or moderate anisotropy (*g*) factor values. Due to the same reason, the previously studied supramolecular systems *anti*-**1·L**$_2$ do not exhibit noticeable optical activity in the visible spectral region, and thus are not suitable for study of the chiroptical properties of Q-bands. However, the highly effective chirogenesis observed in **1·L** allows the chiral properties of the corresponding Q transitions to be investigated in detail.

At first, steady-state absorption and fluorescence spectra of **1·L** are analyzed. Hence, in the absorption spectrum of the tweezer **1·2$_{R,R}$**, besides above-mentioned enhancement of the Q_{10} transition relative to the Q_{00} transition, there is another appreciable difference in comparison to the spectrum of unbound **1** which is reduction of the 0−0 transition splitting from 514 cm^{-1} (for **1**) to 198 cm^{-1} (for **1·2$_{R,R}$**) and sharpening of the Q_{10} band (Figure 6a). It should be realized that, although the two electronic transitions of the monomeric zinc porphyrins possessing D_{4h} symmetry (such as octaethylporphyrin) are degenerate, introduction of the alkyl substituents to the meso position of mono- or bis-porphyrins causes breakdown of this degeneracy, thus resulting in splitting or broadening of the corresponding absorption bands.[24] It is notable that the above-mentioned decrease in the energy difference between the corresponding transitions is achieved by simultaneous bathochromic and hypsochromic shifts of the high and low energy components of the Q_{00} band (and apparently Q_{10} band). Similar tendencies are also seen in the fluorescence spectra. In particular, the emission Q^*_{00} and Q^*_{01} bands of **1·2$_{R,R}$** show a substantial shift to shorter wavelengths by 20 nm compared to those of **1** (Figure 6b), elevating the lowest excited-state energy (E_{00}) of the tweezer by 287 cm^{-1} with simultaneous decreases in the Stokes shift by 451 cm^{-1}. These changes of spectral and photophysical parameters

(23) (a) Tashiro, K.; Konishi, K.; Aida, T. *J. Am. Chem. Soc.* **2000**, *122*, 7921. (b) Barnes, N. R.; Schreiner, A. F.; Dolan, M. A. *J. Inorg. Biochem.* **1998**, *72*, 1. (c) Liu, H.-y.; Huang, J.-w.; Tian, X.; Jiao, X.-d.; Luo, G.-T.; Ji, L.-n. *Inorg. Chim. Acta* **1998**, *272*, 295. (d) Mizutani, T.; Ema, T.; Yoshida, T.; Renné, T.; Ogoshi, H. *Inorg. Chem.* **1994**, *33*, 3558.

(24) (a) Chernook, A. V.; Shulga, A. M.; Zenkevich, E. I.; Rempel, U.; von Borczyckowski, C. *J. Phys. Chem.* **1996**, *100*, 1918. (b) Zen'kevich, E. I.; Shul'ga, A. M.; Gurinovich, G. P.; Sagun, E. I.; Chernook, A. V. *Zh. Prikl. Spektrosk.* **1985**, *42*, 207.

are in good agreement with the observed enhancement of structural rigidity and conformational stability of the tweezer structure **1·L** in comparison to nonligated bisporphyrin **1**. In general, ground (S_0) and excited (S_1) states differ from each other in geometry and the status of the solvation shell of the chromophores. These variations produce a Stokes shift, that is the energy difference in the absorption and emission from the lowest vibrational levels of S_0 and S_1 states. More conformationally rigid systems require less structural reorganization in the relaxation process, thus producing smaller Stokes shifts. As a consequence of a decrease in vibrational relaxation paths in the excited state, emission takes place from a level quite close to the S_1 Franck−Condon state to a level lying just slightly above the equilibrium S_0 state, resulting in an increase in energy of the emitted quantum relative to more flexible systems, so that the displacement of emission bands towards shorter wavelengths is clearly observed in the case of the structurally rigid **1·2$_{R,R}$**. Similar changes are often seen upon decreasing of the conformational freedom and molecular mobility of monomeric and dimeric porphyrins in frozen glassy solutions or ordered media.[25]

Reflecting the high optical activity of the tweezer complexes **1·L** in the B band spectral region, the Q transitions of **1·2$_{R,R}$** also exhibit CD signals (Figure 6a). However, in contrast to the highly intense negative bisignate couplet of the B band, the Q-bands are less intense and have monosignate profiles of the same negative sign, which is apparently due to the low oscillatory strength of these transitions for exciton coupling. Indeed, there are several examples of similar behavior upon chirogenesis in various porphyrins.[23] It is noteworthy that chirality induction in the Q_{00} and Q_{10} bands is not equivalent although this would be expected for electronic transitions of similar origin, with the Q_{00} transition exhibiting a significant predominance, which is unexpected in light of the Q_{10} band's more intense UV−vis absorption. Analogously in the CPF spectrum of **1·2$_{R,R}$** a negative signal corresponding to the Q^*_{00} transition is the major contribution into the optical activity of the emitted light (Figure 6b). In general, the rotatory strength, R_{fi}, for the transition between the states i and f is given as the imaginary part of the scalar product of electric and magnetic transition moments

$$R_{fi} = Im(<i|\mu_e|f>\cdot<f|\mu_m|i>)$$

where μ_e and μ_m are electric and magnetic dipole moments, respectively. Thus, to obtain an appreciable R_{fi} value for a given transition, both the electric and magnetic transition moments should be non-zero. In the present case, the only difference between the Q_{00} and Q_{10}, or Q^*_{00} and Q^*_{01} transitions is the vibrational level involved ($v = 0$ or 1), which is therefore inferred to be responsible for the contrasting CD and CPF behavior of the Q_{00} and Q_{10} bands, although further theoretical studies are obviously needed to fully elucidate the mechanism and origin of this intriguing phenomenon. However, importantly, both the fluorescence and absorption g factors are relatively large for porphyrin-based systems in solution[4a] and correlate well with each other (2.7×10^{-3} and 3.0×10^{-3}, correspondingly). These results clearly indicate a structural similarity of **1·L** in the S_0 and S_1 states due to the enhanced rigidity of the tweezer complex, which is paramount for high optical activity, while independent of the electronic state involved.

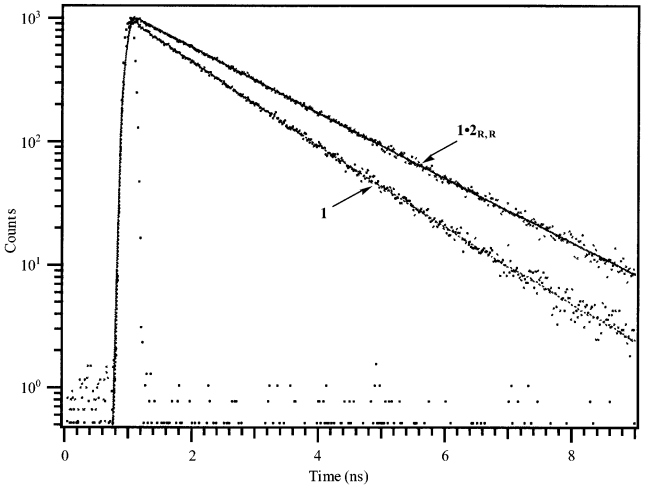

FIGURE 7. Fluorescence decay profiles of **1** and **1·2$_{R,R}$** in CH_2Cl_2 at 292 K.

Additional evidence for the conformational stability of **1·L** in the excited state is obtained from measurements of the fluorescence decay kinetics (Figure 7). Hence, although both **1** and **1·2$_{R,R}$** show monoexponential fluorescence decay profiles, the corresponding lifetimes (τ_f) are distinctly different being 1.22−1.26 ns and 1.61−1.62 ns, respectively, regardless of the monitoring spectral (Q^*_{00} or Q^*_{01}) regions and with χ^2 values less than 1.3. This increase of the τ_f values is caused by the specific spatial arrangement of the tweezer structure where the two porphyrin π electron systems are farther apart from each other in comparison to **1** due to ligand insertion. This hinders inter-porphyrin electronic communication in the tweezer, thus forcing the two porphyrin moieties to behave more like individual chromophores with a lifetime close to the τ_f values of monomeric porphyrin.[26]

6. ^{1}H NMR Spectral Properties. After detailed investigation of **1·L** by optical spectroscopy, the methods of ^{1}H NMR spectroscopy can be applied for further characterization of the tweezer structures, the unique architecture of which should lead to remarkable ^{1}H NMR properties. Importantly, this approach makes it possible to analyze more quantitatively the spatial host−guest arrangement in the tweezer complexes.

To avoid undesirable influence of the 1:2 anti-**1·L$_2$** complexes only the tweezer-forming ligand **2** is used to study the ^{1}H NMR properties of the tweezers.

6.1. 1D and 2D ^{1}H NMR Spectra. The ^{1}H NMR spectra were recorded at room temperature (296 K) and at the **1** to **2$_{R,R}$** molar ratio of 1:1 (in the case of the complex **1·2$_{R,R}$**) to ensure the optimal measuring conditions and shift of the total equilibrium giving over 99% of the corresponding tweezer **1·L**. The 1D spectral profile

(25) (a) Anikin, M. V.; Borovkov, V. V.; Ishida, A.; Wasa, K.; Sakata, Y. *Chem. Phys. Lett.* **1994**, *226*, 337. (b) Takahashi, K.; Hase, S.; Komura, T.; Imanaga, H.; Ohno, O. *Bull. Chem. Soc. Jpn.* **1992**, *65*, 3358. (c) Gurinovich, G. P.; Zenkevich, E. I.; Sagun, E. I.; Shulga, A. M. *Opt. Spectrosc. (USSR)* **1984**, *56*, 637.

(26) The τ_f values of the ZnOEP/Py system in $CHCl_3$ are 1.52−1.54 ns.

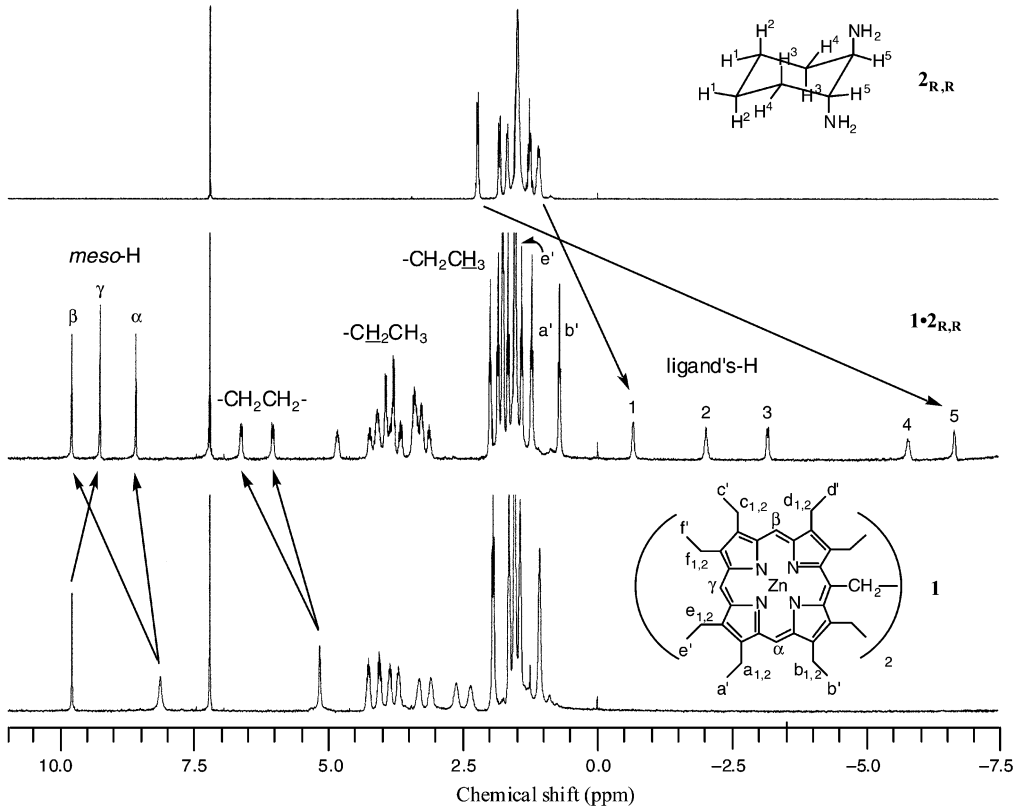

FIGURE 8. ^{1}H NMR spectra of **1·2$_{R,R}$**, **1**, and **2$_{R,R}$** in $CDCl_3$. The subscript 1 indicates the closest $-CH_2CH_3$ proton of **1** and **1·2$_{R,R}$** to the corresponding meso proton, while the subscript 2 indicates the furthest $-CH_2CH_3$ proton to the corresponding meso proton.

of **1·2$_{R,R}$** differs significantly from the initial spectra of **1** and **2$_{R,R}$** (Figure 8 and Supporting Information Figure S4). The most intriguing feature of the ^{1}H NMR spectrum of **1·2$_{R,R}$** is the extraordinarily large upfield shifts of the ligand's protons H^5 ($\Delta\delta = 8.9$ ppm) and NH_2 (up to −7.69 ppm), arising from their proximity to both of the porphyrin subunits and therefore the strong effect of the ring currents. All other ligand's protons are also shifted upfield though to a lesser degree. The order of shifts: $NH_2 > H^5 > H^4 > H^3 > H^2 > H^1$ correlates well with the geometry of the complex and the close proximity of the ligand protons to the porphyrin planes, as can be seen on a CPK model (see **1·2$_{R,R}$** in Figure 3). Similar but smaller shifts of the guest's protons clamped between the porphyrin subunits have been also observed in various tweezer systems.[7a,d,e,g,8b,f−h] In sharp contrast to these upfield shifts, protons of the porphyrin's subunits ($-CH_2$-CH_2-, 10,20-*meso*-H, $-CH_2CH_3$) are noticeably downfield-shifted due to conformational changes upon tweezer formation, which result in moving the two porphyrin rings farther apart from each other and subsequently decreasing the shielding effect of the neighboring porphyrin observed in the face-to-face *syn*-**1**. Furthermore, these protons become nonequivalent in the chiral tweezer as a result of their different exposure to the ring-current effect. The largest split of 1.20 ppm is found for the 10,-20-*meso*-H, which are most affected by the anisotropy of the neighboring porphyrin, while H_A and H_B of the $-CH_2$-CH_2- bridge protons are split moderately by 0.59 ppm. It should be also noted that in the case of $-CH_2CH_3$ groups, the biggest nonequivalence of 0.69 and 0.44 ppm is observed for the corresponding geminal $h_{1,2}$ and $g_{1,2}$, protons, which are closest to the neighboring porphyrin. Splitting of other methylene protons is in good agreement with the left-handed helicity of **1·2$_{R,R}$**. In this screw structure the $b_{1,2}$, $a_{1,2}$, and $e_{1,2}$ protons of one porphyrin subunit locate above the π-electron system of the second porphyrin, thus inducing noticeable differences between the corresponding signals ranged from 0.25 to 0.11 ppm, while the more distant $d_{1,2}$, $c_{1,2}$, and $f_{1,2}$ protons show negligibly small (0.08−0.01 ppm) or no splits.

Additional important structural information along with full assignment of the corresponding proton resonances is obtained from the 2D ^{1}H−^{1}H COSY (Figure S5, Supporting Information) and ROESY spectra (Figures S6 and S7, Supporting Information).

In particular, observation of the positive ROE cross-peaks in the ROESY spectrum of **1·2$_{R,R}$** due to through-space interactions between the ligand's protons and the porphyrin *meso* and $-CH_2CH_3$ protons unambiguously supports the tweezer structure. Furthermore, these ROEs arise from the porphyrin protons (α, γ, a′, b′, e′) locating on only one edge of the macrocycle, which faces towards the second porphyrin. This indicates a stereospecific manner of the through-space interactions in accordance with the screw handedness of **1·2$_{R,R}$** and a central disposition of the guest molecule inside the host that is ensured by two well orientated Zn−N coordination bonds.

6.2. Determination of the H−H Distances. Besides the more qualitative description of the spatial arrangement of **1·2$_{R,R}$** in section 6.1, the ^{1}H NMR spectroscopy allows a more quantitative structural analysis of the

tweezer by applying the selective relaxation method to determine the corresponding interproton distances. This method is based on the measurement of two kinds of T_1 value (T_1^{NS} and T_1^{SNI}) followed by treatment according to the procedure described above (see the Experimental Section and Scheme 1).[9]

The observed T_1^{NS} values of $\mathbf{1{\cdot}2_{R,R}}$ are obtained at 200 and 500 MHz (see Table S8, Supporting Information), where the values at 500 MHz are larger than those at 200 MHz exhibiting clear frequency dependence. From eq 6 (see the Experimental Section), the calculated plot of τ_c versus the ratio $T_1^{NS}(500)/T_1^{NS}(200)$ is obtained (Figure S9, Supporting Information) and the corresponding τ_c values for several protons are evaluated using this plot (Table S8, Supporting Information). The correlation times are rather large, even for the ligand, and this suggests slow molecular motion of the guest molecule, thus supporting the tweezer structure, in which the ligand is squeezed between two porphyrin rings.

The observed T_1^{SNI} values for several meso protons of the porphyrin moiety and ligand's protons were obtained at 500 MHz and are listed in Table S10 (see the Supporting Information). Essentially, the porphyrin protons excepting the meso protons show too short T_1 values to give the accurate interproton distances. Since the σ_{ij} values are obtained from the difference of the reciprocals of two different T_1 values (as mentioned above), some problems of precision arising from the relatively short T_1 or small σ_{ij} values are minimized by averaging the repeated measurements.

For some protons the T_1^{SNI} values are larger than the T_1^{NS} values resulting in greater σ_{ij}, values, and thus indicating shorter distances between protons i and j. Based on both T_1 values, the experimental σ_{ij} values are estimated from eq 5 (see Table S11, Supporting Information). Using the σ_{ij} and τ_c values and eq 4, the r_{ij} values are obtained and summarized in Table S12 (Supporting Information).

For each proton pair in a porphyrin ring, only one value of σ_{ij} from the corresponding meso proton is estimated thus giving only one value of r_{ij}, while in the case of the porphyrin-ligand and ligand protons pairs two values σ_{ij} and σ_{ji} are obtained, thus leading to a range of the r_{ij} values. The interproton distances obtained for the individual porphyrin and ligand parts of $\mathbf{1{\cdot}2_{R,R}}$ are credible and correlate well with those obtained from the corresponding MM2 molecular mechanics calculations of the molecules **1** and $\mathbf{2_{R,R}}$ (not shown). Although only two interproton distances between the porphyrin and ligand parts were determined (α-5 = 3.5 Å and β-2 = 3.0−3.3 Å), they further support the tweezer structure of $\mathbf{1{\cdot}2_{R,R}}$, where the ligand part is fixed at short distance between the two porphyrin rings.

7. ESI MS Spectral Properties. As additional support for formation of the stable 1:1 complexes during supramolecular chirogenesis in **1** upon interaction with bidentate ligands, ESI MS experiments were carried out to detect and characterize all equilibrium species. As in the case of monodentate ligands,[4b] to reduce the signal-to-noise level variable temperature measurements at a fixed host−guest molar ratio were chosen as the most suitable approach; the same samples used for the ^{1}H NMR experiments were applied to the study of the complexation process by ESI MS. Representative examples are shown in Figure 9 for $\mathbf{2_{R,R}}$ and $\mathbf{3_{R,R}}$. Thus, while in the spectrum of **1** there is only a signal associated with the corresponding molecular ion $[\mathbf{1}]^+$, addition of 1 equiv of $\mathbf{2_{R,R}}$ results in the appearance of a new peak attributed to formation of a 1:1 complex $[\mathbf{1{\cdot}L}]^+$ at 110 °C. Lowering the temperature to 90 °C increases the relative intensity of the $[\mathbf{1{\cdot}L}]^+$ signal due to enhancement of the ligand binding strength as also found for monodentate ligands.[4b] There is no indication of the peak associated with a 1:2 complex, thus showing exclusive formation of the **1·L** species and agreeing well with other spectral data reported in previous chapters.

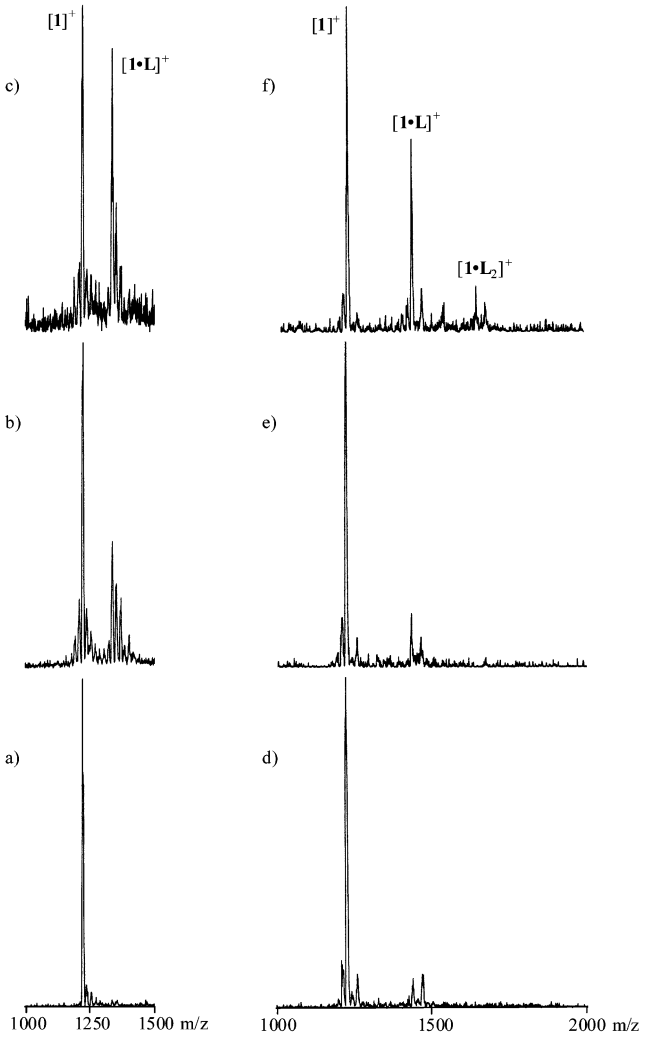

FIGURE 9. Selected areas of the ESI mass spectra of **1** in $CDCl_3$ without external ligand at 110 °C (a) and in the presence of $\mathbf{2_{R,R}}$ in $CDCl_3$ at 110 °C (b) and 90 °C (c) and $\mathbf{3_{R,R}}$ in CH_2Cl_2 at 110 °C (d), 90 °C (e), and 70 °C (f).

In sharp contrast to $\mathbf{2_{R,R}}$, the MS behavior of $\mathbf{3_{R,R}}$ is dramatically different (Figure 9d−f). Although initially the spectral pattern upon addition of $\mathbf{3_{R,R}}$ is similar to that of $\mathbf{2_{R,R}}$ showing the peaks of $[\mathbf{1}]^+$ and $[\mathbf{1{\cdot}L}]^+$, further decrease of the temperature results in the appearance of a signal associated with the 1:2 complex $[\mathbf{1{\cdot}L_2}]^+$ due to the second equilibrium step as observed by optical spectroscopy (although the decrease in temperature also, unavoidably, results in an increase of the noise level). Interestingly, the ratio of molecular peak intensities of the 1:1 and 1:2 complexes showed $[\mathbf{1{\cdot}L}]^+$ being 4.2 times

higher than that of $[\mathbf{1}\cdot\mathbf{L}_2]^+$, correlating well with the large difference in free energy change observed for the corresponding 1:1 and 1:2 complexes ($\Delta\Delta G = 5.5$ kcal mol^{-1}).

Conclusions

This work clearly demonstrates effective supramolecular chirogenesis in the achiral bis-porphyrin host upon noncovalent interactions with bidentate chiral guests containing amino/hydroxyl groups, which are able to coordinate to the central zinc ion of the porphyrin. This process is based on a multistep equilibrium, which includes two major steps: first, ligand binding to the syn form of bis(zinc porphyrin) leading to destruction of the strong $\pi-\pi$ interporphyrin interactions and producing the tweezer structure; and second, binding of a second ligand generating the 1:2 anti complex. All experimental data obtained by various spectroscopic methods agree well with this model. The quantitative analysis of the experimental titration data using the standard least-squares fitting procedure reveals that the first binding is significantly stronger than the second. The guest-binding strength is dependent upon the nature of the ligand's substituents and corresponding functional groups. The general tendencies of the complexation process are as follows. Diamines have greater affinity than amino alcohols; bulkier aromatic containing ligands bind more weakly than less bulkier aliphatic amines; increase of the complexes steric hindrance (e.g., via enlargement of the ligand's substituents or a less favorable spatial arrangement of the binding groups) results in reduction of the tweezer formation and switching of the complexation pathway to form the 1:2 complex. It was found that the enhanced conformational stability and optimal geometry of the tweezer complex ensures efficient transfer of chirality information from a chiral guest to the achiral host, inducing extraordinary optical activity in the supramolecular system. Moreover, a remarkable and rarely observed example of stoichiometry controlled chirogenesis was observed for certain supramolecular systems.

The results obtained offer a clearer insight into the total mechanism of supramolecular chirogenesis in natural and artificial systems, and may have practical implications in the design of chiroptical molecular devices. Specifically, a high chiroptical sensitivity of the host molecule to external guest molecules makes it possible to use this system as an effective chiral sensor. Further studies to enhance the applicability and sensitivity of this system for other types of chiral compounds are currently in progress, and will be the subject of future reports from our group.

Acknowledgment. We thank Mr. M. Abe for technical support with the ESI MS measurements and Dr. A. Nakamura and Dr. S. Taniguchi for assistance with fluorescence measurements.

Supporting Information Available: Additional UV−vis, CD, and ^{1}H NMR spectral data. This material is available free of charge via the Internet at http://pubs.acs.org.

JO034814K